4. Basic Segments of Pulse Sequences

The first applications of 2D NMR for studies of proteins in aqueous solution used only very few pulse sequences [5–7]. Today, a vast number of experimental schemes exist and new ones are continuously developed. Fortunately, a pulse sequence usually consists of a number of portions which belong to a rather small group of key segments from which most experimental schemes can be constructed. Many of the basic segments can be described in the framework of the operator formalism for spin $\frac{1}{2}$ nuclei [28]. For segments based on relaxation or strong spin-spin coupling, for example NOESY or TOCSY mixing periods, more extensive quantum mechanical treatments have to be applied. Once the key segments are characterized they can be used to sequentially analyse complex pulse sequences segment by segment.

Fig. 10 shows a pulse sequence diagram which shall serve as an example to illustrate that a pulse scheme is constructed from a limited number of basic segments. Above the pulse sequence the individual basic segments are indicated with a short description and a number in brackets indicating the figure which describes the corresponding segment in more detail. For example the transfer of magnetization from one nuclear species to another is used six times in this sequence. In the pulse scheme narrow and wide black vertical bars represent 90^o and 180^o *rf* pulses which are drawn on different horizontal lines for different frequencies. In this example the resonance frequencies for proton (H), nitrogen (N), carbonyl carbon (C') and α-carbon (C) nuclei are shown. An additional horizontal line labelled G indicates where pulsed magnetic field gradients are applied. The first 90^o *rf* pulse on H excites proton magnetization and at the very end of the sequence during the period t_3 proton magnetization is detected. The experimental scheme correlates the chemical shifts of the amide proton and nitrogen (HN) with the α-carbon chemical shift (CA) of the preceding residue in the amino acid sequence *via* the intervening carbonyl carbon (CO). This 3D experiment is called HN(CO)CA [139, 140] which is an acronym that summarizes the magnetization transfer and the nuclei from which the chemical shift is measured. A cross peak in the corresponding 3D spectrum indicates a connection *via* the peptide bond of two sequential amino acids in a fully $^{15}N/^{13}C$ enriched protein. Hence the experiment facilitates the sequential assignment of all amino acid spin systems in a protein. A detailed discussion of the HN(CO)CA experiment can be found in the original publications [69, 139, 140], but for the present purpose a brief summary suffices. The sequence starts with the excitation of amide proton magnetization which is subsequently transferred to the attached ^{15}N nucleus whose chemical shift is measured during t_1. Next the magnetization is transferred *via* the C'-carbon of the preceding residue to that residues α-carbon whose chemical shift is measured during t_2. Subsequently the magnetization is transferred back to the ^{15}N nucleus of the original residue *via* the C'-carbon and finally to the amide proton where it originated. During the period t_3 the amide proton signal is measured.

In the following, commonly used key segments are analysed on the basis of a two spin system with the scalar coupled spins *I* and *S*. Strong spin-spin coupling is not considered unless absolutely necessary, for example in TOCSY sequences. The key segments which are discussed in this section are visually represented by pulse sequence diagrams which all use the same conventions (*e.g.* Fig. 11 and Fig. 12). Thin and wide black vertical bars on the horizontal lines labelled I and S stand for 90^o and 180^o *rf* pulses applied to the *I* or *S* spin, respectively. All *rf* pulse have phase x unless indicated otherwise at the top of the pulse bars. The excitation pulse in the sequences is omitted and must be added when applying the segment to *z* states of the spin system. The resonance frequency of *I* and *S* are denoted ω and Ω, respectively. For strictly homonuclear segments *I* and *S* are assigned to only one line labelled I/S (*e.g.* Fig. 13). Decoupling and *rf* mix-

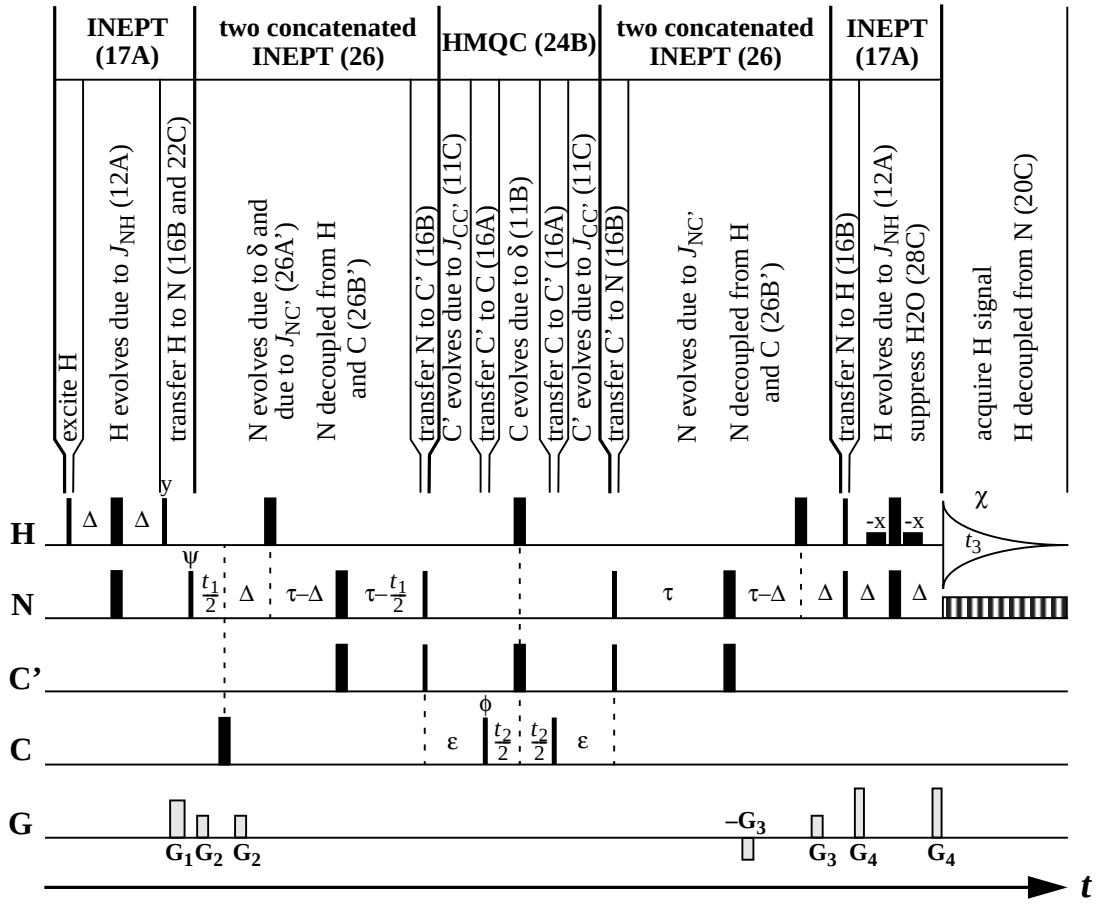

Fig. 10. Experimental scheme for the HN(CO)CA experiment [139, 140] used to illustrated the segmentation of a pulse sequence into a limited number of different basic segments. The vertical lines above the pulse sequence indicate start and end of individual basic segments of the pulse scheme. The text between these lines describes the action of the particular segment and the number in brackets indicates the figure in the main text that shows the corresponding segment. At the very top common combinations of key segments (Section 4.5), for example INEPT, are indicated with the number of the figure in brackets where they are discussed. The abbreviations H, N, C' and C stand for the amide proton, the nitrogen, the carbonyl carbon and the α-carbon nuclei. J_{NH}, $J_{NC'}$ and $J_{CC'}$ represent the scalar coupling constant between N and H, N and C' and C and C', respectively, δ stands for chemical shift. In the pulse scheme narrow and wide black vertical bars represent 90^o and 180^o *rf* pulses which are indicated on different horizontal lines for different frequencies: H, N, C' and C stand for the resonance frequencies of the H, N, C' and C nuclei, respectively. All *rf* pulses are applied with phase x unless indicated otherwise on top of the pulse bars where ψ stands for the phase cycle x, x, –x, –x, ϕ for x, –x and χ for the receiver cycle x, –x, –x, x. Pulsed magnetic field gradients (PFGs) are indicated on a separate horizontal line labelled G and PFGs with the same label G_i have the same strength and duration which differ from all other PFGs. The time periods t_1, t_2 and t_3 denote the three chemical shift evolution periods. The time periods labelled Δ, τ and ε are necessary to prepare the correlation between different nuclei and have the values $\Delta = (4J_{NH})^{-1}$, $\tau = (4J_{NC'})^{-1}$ and $\varepsilon = (2J_{CC'})^{-1}$.

ing sequences are indicated by striped rectangles (*e.g.* Fig. 11 and Fig. 14). To indicate pulsed field gradients an additional horizontal line G is added to the sketches (*e.g.* Fig. 22) and PFGs are indicated by grey rectangles. Rarely used graphical objects are explained in the figure legends. Together with the figures there are tables provided which summarize the transformation properties of the key segments using the product operator formalism. Preference is given to a description using the shift operator basis which allows a more compact formulation of evolution due to

chemical shift and magnetic field gradients. In some instances operators in both basis systems are indicated facilitating the link between the currently more commonly used cartesian basis and the shift operator basis. Cartesian operators are used only in cases when they allow a much more compact description.

4.1 Evolution segments

Evolution segments consist of a time period *t* during which the spin system evolves essentially free from external *rf* disturbances except possibly one or two 180^o pulses (Fig. 11). During *t* transverse magnetization components evolve due to their chemical shift and *J* coupling. Typical examples which use evolution segments are the incremented time periods introduced in pulse sequences to obtain multidimensional NMR experiments or the fixed time periods used for the preparation of in-phase and anti-phase spin states in heteronuclear experiments. Evolution segments can easily be analysed using the product operator formalism. Fig. 11 shows different chemical shift evolution segments and Table 4 presents the transformation properties of typical two-spin states when submitted to these sequences. In multidimensional experiments the time period *t* in these sequences may be incremented during an experiment to sample frequencies in indirect dimensions. When a 90^o pulse at the start of the evolution segment brings *z* magnetization into the transverse plane the effective evolution of these magnetization components due to the chemical shift has a longer duration than indicated by *t*. This is a consequence of the non-ideal behaviour of *rf* pulses (see Appendix). Resonance lines with an offset ν_k from the carrier frequency acquire a phase error in units of radians of $4\tau_{90}\nu_k$ during a 90^o pulse with duration τ_{90} and strength γB_1 [16, 24, 26]. The linear offset dependence of the phase error holds as long as ν_k is less than γB_1 [16]. Hence, an off-resonance 90^o pulse can be treated as an ideal pulse followed by an evolution period given by $t_o = 2\tau_{90}/\pi$. Similarly rotating transverse magnetization to the *z* axis can be treated as an ideal pulse preceded by a delay $t_o = 2\tau_{90}/\pi$ [141]. Thus there is an effective increase of *t* by t_o or $2t_o$ depending on whether the evolution segment is bound by one or two 90^o pulses, respectively. When evolution segments are used in multidimensional experiments to sample the resonance frequencies in indirect dimensions this inherent evolution time leads to a linear phase gradient of the signals which can be corrected by a first order phase correction. However, a linear phase correction may introduce baseline curvature [97, 99] and should be avoided unless the correction is an exact multiple of 180^o which leaves the baseline unaffected. Consequently the initial evolution time t_{ini} in the indirect dimension is often set to half a dwell time which results in a linear phase dependence of 180^o across the spectrum. The inherent evolution time can then be compensated by a subtraction from t_{ini}. An additional benefit is that folded peaks in such a spectrum have opposite sign simplifying their identification.

Fig. 11B presents a segment where the net evolution of the *I* spin at the end of the period *t* does not depend on the scalar coupling *J*. The state of spin *I* at the end of *t* is unaffected by the coupling with *S* spins. Fig. 11C depicts a segment where the state of *I* at the end of *t* is unaffected by chemical shift and J coupling and has effectively only been inverted by the 180^o pulse. In practical implementations the performance of the sequences in Fig. 11B and C may suffer due to the limited inversion and refocusing profiles obtained for real 180^o pulses which may introduce artifacts in the final spectrum. A 180^o pulse with strength γB_1 inverts for example only 80% of the *z* magnetization at an offset as small as $0.3\ \gamma B_1$ and at the same offset it refocuses less than 85% of *x* magnetization when applied along the *x* axis (Fig. 7). The inversion profile can be substantially improved using simple composite pulses, a solution which is not available for refocusing pulses (Section 2.2.1). Imperfect pulses result not only in a loss of sensitivity but in addition unwanted

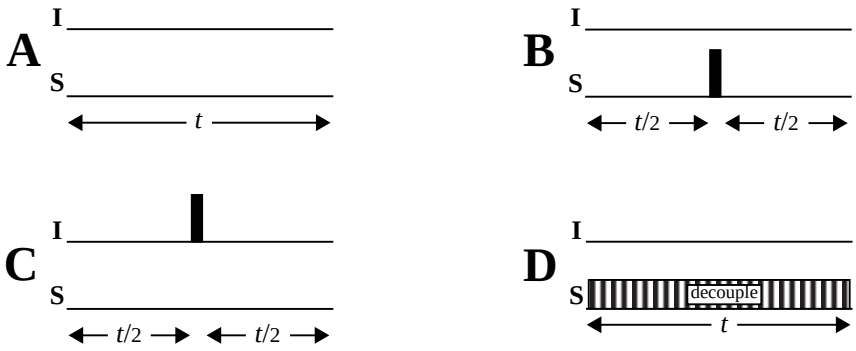

Fig. 11. Schemes for typical segments used to allow spins *I* to evolve due to chemical shift and/or *J* coupling for example in multidimensional NMR pulse sequences. The spins *I* evolve due to chemical shift in sequences A, B and D, and in sequence A in addition due to scalar coupling to the *S* spins. Table 4 presents the transformation properties of these sequences.

Table 4
Evolution due to chemical shift and/or *J* coupling

Fig. 11	initial state	resulting product operators describing the transformation properties of the sequence
A	I^+	$I^+\cos(\pi Jt)\,e^{-i\omega t} - 2iI^+S_z\sin(\pi Jt)\,e^{-i\omega t}$
	$2I^+S_z$	$2I^+S_z\cos(\pi Jt)\,e^{-i\omega t} - iI^+\sin(\pi Jt)\,e^{-i\omega t}$
	$2I^+S^+$	$2I^+S^+\,e^{-i(\omega+\Omega)t}$
B	I^+	$I^+\,e^{-i\omega t}$
	$2I^+S_z$	$-2I^+\,S_z\,e^{-i\omega t}$
	$2I^+S^+$	$2I^+S^-\,e^{-i\omega t}$
C	I^+	I^-
	$2I^+S_z$	$2I^-S_z$
	$2I^+S^+$	$2I^-S^+\,e^{-i\Omega t}$
D	I^+	$I^+\,e^{-i\omega t}$
	$2I^+S_z$	0
	$2I^+S^+$	0

peaks may appear in the final spectrum. In evolution periods of multidimensional NMR experiments the EXORCYCLE (Section 2.2.1) should be used to prevent the appearance of artifact peaks in the final spectrum, alternatively pulsed field gradients fulfil the same purpose (Section 4.4). For the segment in Fig. 11B the alternative sequence in Fig. 11D can be used which maintains the decoupled state of *I* throughout the period *t* by the application of a decoupling sequence (Section 4.3).

Fig. 12 presents typical pulse sequence segments used to prepare and/or select special spin states obtained from evolution due to scalar couplings. The segment in Fig. 12A transforms in-phase into anti-phase magnetization or vice versa depending on the initial state (Table 5). The total evolution time period τ is kept fixed and the application of a 180^o to both spins refocuses the chemical shift of the *I* spins but maintains the evolution due to scalar coupling. This sequence finds its application typically in heteronuclear experiments where nuclei of different species are brought into an anti-phase state to prepare a coherence transfer or where magnetization is refocused from an anti-phase state after a coherence transfer step to obtain observable magnetization. To counteract relaxation the delay τ is usually set to values shorter than the optimum of $(2J)^{-1}$ needed for complete evolution into anti-phase magnetization. In practical implementations the performance of the 180^o pulses requires special attention to avoid artifacts in the spectrum and the discussion in conjunction with Fig. 11B and C is valid here as well.

Evolution due to *J* coupling is also used to prepare states which differ in sign allowing a separation of signals from species where nuclei *I* are bound to a nucleus *S* from those where nuclei *I* are not bound to a nucleus *S* (Fig. 12B and C) [142, 143]. Using this segment, for example, protons *I* bound to a ^{15}N nucleus can be separately observed from protons *H* not bound to ^{15}N. For the separation of the two classes of nuclei the segment is applied twice, once with a 180^o and once without a 180^o pulse on the *S* spins. For both the filter element (Fig. 12B) and the half filter element (Fig. 12C) the difference of the two signals thus obtained selects resonances of the nuclei which are bound to a heteronucleus and for the half filter the sum selects the resonances of the nuclei not bound to a heteronucleus [143]. Half filter experiments can for example be used to observe the interaction of the amide protons separately from those of the aromatic protons in a homonuclear 2D experiment of a ^{15}N labelled protein. In a further application, nuclei from two different molecules in a sample can be observed in two separate spectra when one molecule is labelled with a heteronucleus *S* and the other is not [144, 145].

In practice two 90^o pulses are used to form the 180^o pulse on the *S* nuclei (Fig. 12B and C). Two experiments are performed, one with the same *rf* phase for the two 90^o pulses to produce a 180^o pulse and one with a phase difference of 180^o for the two 90^o pulses producing an effective 0^o pulse. The reason for this technical trick lies in the poor inversion profile of the 180^o pulse. The 90_x90_{-x} pulse sandwich results only in a 0^o degree pulse on resonance, off-resonances it shows an excitation profile that very closely matches the inversion profile of a 180^o pulse in the frequency range $\pm\gamma B_1$. Hence, the 90_x90_{-x} pulses compensate the non-ideal behaviour of the 180^o pulse and reduces signal contributions from the *I* spins when non-bonded *H* spins are to be selected. This technique improves the selection of *H* spins but spurious signals of *I* resonances still constitute a permanent problem [143]. Not only must the 180^o pulse invert all the *S* spins, but the filter delay must exactly match $(2J)^{-1}$. The latter condition often cannot be fulfilled since the values of the coupling constants vary particularly if the heteronucleus is ^{13}C. In addition the labelling fraction of the *S* nuclei must be 100% otherwise breakthrough cannot be prevented. In contrast to the problems with the selection of the *H* resonances the selection of the *I* resonances usually constitutes no problem because imperfections do not introduce *H* spin resonances but merely reduce the *S/N* of the selected *I* resonances. This discussion of filter elements with two spins qualitatively applies to systems with more spins as long as the heteronuclear coupling constants are much larger than the homonuclear coupling constants among the *I* and *H* spins and among the *S* spins [143].

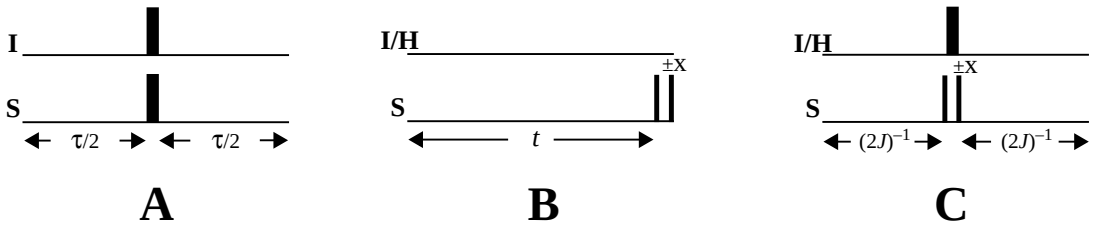

Fig. 12. Typical schemes for the preparation of spin states based on their evolution due to scalar coupling. Sequence A transforms in-phase *I* magnetization into *I* magnetization in anti-phase to spin *S* and vice versa. B and C allow to separate spins *I* which are bound to spin *S* from those *I* spins (H) which are not bound to *S*. This is achieved by properly adding or subtracting two scans, I and II (Table 5), with phase x and –x for the second 90° pulse applied to the *S* spins. Table 5 presents the transformation properties of these sequences.

Table 5
Preparation/selection of states based on their evolution due to *J* coupling

Fig. 12	initial state†	resulting product operators describing the transformation properties of the sequence‡
A	I^+	$2i\, I^- S_z \sin(\pi J\tau) + I^- \cos(\pi J\tau)$
	$2I^+S_z$	$-i\, I^- \sin(\pi J\tau) - 2I^- S_z \cos(\pi J\tau)$
	$2I^+S^+$	$2I^- S^-$
B	$I^+ + H^+$	$(I) + (II) = 2I^+ \cos(\pi Jt)\, e^{-i\omega(I)t} + 2H^+ e^{-i\omega(H)t}$
	$I^+ + H^+$	$(I) - (II) = 4i\, I^+ S_z \sin(\pi Jt)\, e^{-i\omega(I)}$
	$H^+ + 2I^+S_z$	$(I) + (II) = -2i\, I^+ \sin(\pi Jt)\, e^{-i\omega(I)t} + 2H^+ e^{-i\omega(H)t}$
	$H^+ + 2I^+S_z$	$(I) - (II) = -4\, I^+ S_z \cos(\pi Jt)\, e^{-i\omega(I)}$
C	$H^+ + I^+$	$(I) + (II) = 2H^-$
	$H^+ + I^+$	$(I) - (II) = -2\, I^-$
	$H^+ + 2I^+S_z$	$(I) + (II) = H^- + 2I^- S_z$
	$H^+ + 2I^+S_z$	$(I) - (II) = 0$

† *I* and *H* stand for the same type of nucleus; the spins *I* are coupled to the spins *S* and the spins *H* are not coupled to S spins, the spins *I* and *H* are not coupled.

‡ (I) stands for the segment where both 90° pulses on *S* spins are applied with phase x and (II) for the segment with phases x and –x. (I) + (II) represents the sum of the two scans, (I) – (II) the difference; the resonance frequencies of the *I* and the *H* spins are indicated by ω(I) and ω(H), respectively.

4.2 Transfer segments

4.2.1 Homonuclear through-bond transfer

Magnetization transfer between spins is based on through-bond connectivities *via J* couplings, on through-space interactions *via* NOEs and ROEs or on chemical exchange. Transfer segments accomplish magnetization or coherence transfer and establish a correlation between the spins. The simplest transfer segment consists just of a 90^o pulse that acts on homonuclear anti-phase magnetization developed during an evolution time period *t* due to scalar coupling (Fig. 13A). The 90^o pulse acting on anti-phase coherence causes a coherence transfer. This segment was embedded in the first 2D experiment proposed [3, 4] which was later named COSY which stands for 2D correlation spectroscopy [7, 146, 147]. In proteins usually only couplings over a maximum of three chemical bonds are large enough to manifest themselves in a COSY step. In [^{1}H, ^{1}H]-COSY experiments the anti-phase magnetization cannot be refocused due to the widely different coupling constants. In multidimensional spectra anti-phase multiplet signals are thus obtained which contain positive and negative contributions that tend to cancel each other for broad resonance lines. When the coupling constants vary only in a narrow range as for aliphatic carbon coupling constants in ^{13}C labelled proteins, refocusing of the anti-phase magnetization obtained after the transfer step becomes possible and in-phase peaks can be obtain in the spectrum.

The sequence in Fig. 13B is closely related to the COSY sequence and excites multiple quantum coherence [148]. In-phase magnetization evolves into anti-phase magnetization during τ due to scalar coupling. A 180^o pulse refocuses the chemical shift evolution. Setting the phase ϕ of the 90^o pulse at the end of the segment to x results in even-quantum coherences being detected whereas for ϕ = y odd-quantum coherences are obtained [149]. The length of the time period τ, the number of coupled spins and their mutual coupling constants determine the exact states that can be created. Again, the product operator formalism suffices to analyse the sequence (Table 6). Multiple quantum coherences are *n* times more sensitive to magnetic field gradients and phase shifts of *rf* pulses than single quantum coherences and similarly have proportionally larger susceptibility to the effects of pulse imperfections, a fact that may influence the performance of the sequence in practical implementations.

The double quantum filter segment shown in Fig. 13C eliminates coherence pathways which do not pass coherence level |p| = 2 between the two 90^o pulses and are not in the coherence state p = –1 after the second pulse. Hence, coherence order changes Δp of –3 or +1 are selected (Fig. 1). Following the recipe given at the end of Section 2.1.2 the appropriate phase cycling scheme can be designed [38]. With $N = 4$ phase steps of $\Delta\phi = 90^o$ the pulse phase cycle becomes ϕ = x, y, –x, –y and the signal must be accumulated with the receiver cycling through x, –y, –x, y (Fig. 13C, Table 6). More generally a multiple quantum filter consists of two 90^o pulses which are separated by the time to switch the phase of a pulse, typically two microseconds. By proper phase cycling of the phase ϕ of the second pulse the coherence level between the pulses that contributes to the final signal can be selected.

Nuclei separated by more than three chemical bonds but belonging to the same spin system can be correlated using several COSY-steps. Depending on the size of the coupling constants involved this approach may be limited to very few steps by transverse relaxation. Total correlation (TOCSY) mixing sequences (Fig. 14) offer a more efficient scheme where all transfers are active simultaneously and the relaxation depends on a mixture of longitudinal and transverse relaxation rates and is therefore slower than in a COSY-step. In addition the TOCSY sequence

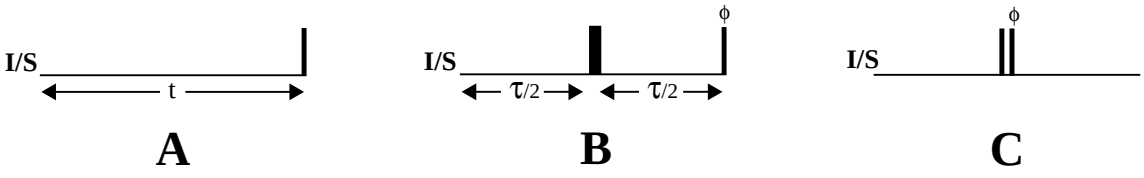

Fig. 13. Schemes of typical homonuclear through-bond transfer segments used in multidimensional NMR pulse sequences. Segment A represents a COSY type transfer. Segment B serves for the creation of multiple quantum states; the phase ϕ allows selection of even or odd multiple quantum coherence to an order which depends on the number of coupled spins. Segment C represents a double quantum filter with ϕ = x, y, –x, –y and the receiver phase x, –y, –x, y; this element selects coherences which pass through a double quantum state between the two pulses. Table 6 presents the transformation properties of these segments.

Table 6
Homonuclear through-bond transfer segments

Fig. 13	**initial state**	**resulting product operators describing the transformation properties of the sequence**[†]
A	I^+ I_y	$(I^- + I^+ + 2iI_z)\ (i(S^- - S^+)\sin(\pi Jt) + \cos(\pi Jt))\ e^{-i\omega t}/2$ $-I_x\cos(\pi Jt)\sin(\omega t) + I_z\cos(\pi Jt)\cos(\omega t) + 2I_xS_y\sin(\pi Jt)\cos(\omega t) +$ $+ 2I_zS_y\sin(\pi Jt)\sin(\omega t)$
	$I^+ S_z$ $2I_yS_z$	$-i(I^- + I^+ + 2iI_z)\ ((S^- - S^+)\cos(\pi Jt) + \sin(\pi Jt))\ e^{-i\omega t}/2$ $-I_x\cos(\omega t)\sin(\pi Jt) - I_z\sin(\omega t)\sin(\pi Jt) + 2I_xS_y\sin(\omega t)\cos(\pi Jt) +$ $- 2I_zS_y\cos(\omega t)\cos(\pi Jt)$
	$2I^+S^+$ $2I_yS_x$	$(I^- + I^+ + 2iI_z)\ (S^- + S^+ + 2iS_z)\ e^{-i(\omega+\Omega)t}$ $-2I_xS_x\cos(\Omega t)\sin(\omega t) + 2I_zS_x\cos(\omega t)\cos(\Omega t) - 2I_xS_z\sin(\omega t)\sin(\Omega t) +$ $+ 2I_zS_z\cos(\omega t)\sin(\Omega t)$
B	I_y	$\phi = x: -I_z\cos(\pi Jt) - 2I_xS_y\sin(\pi Jt)$ $\phi = y: -I_y\cos(\pi Jt) - 2I_z S_x\sin(\pi Jt)$
C	I^+	0
	$2I^+S_z$	$-I_z(S^+ + S^-)/2 - (I^+ + I^-)S_z/2$
	$2I^+S^+$	$I^+(3S^+ - S^-)/4 - I^-(S^+ - 3S^-)/4 + I_zS_z$

[†] For the transformation under the sequence of Fig. 13C the sum of four transients is indicated which is obtained with the phase cycle ϕ = x, y, –x, –y and the concomitant receiver cycling x, –y, –x, y.

also transfers in-phase magnetization in contrast to COSY which transfers only anti-phase magnetization. The TOCSY transfer segment consists of a strong spin-lock mixing sequence [43, 44] (Fig. 14). The different mixing sequences available have rather similar average power require-

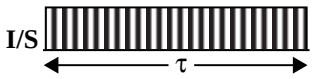

Fig. 14. Scheme for a homonuclear TOCSY transfer segment. During τ the spins *I* and *S* are spin-locked with a strong *rf* field which makes possible magnetization transfer from the *I* to the *S* spin, and vice versa, according to Eq. (2.9).

ments. The choice of the sequence depends on the orientation of the magnetization at the start of the sequence, whether the mixing is applied to protons or other nuclei and the required efficiency of the mixing for magnetization components in the three spatial dimensions. All mixing sequences simultaneously transfer magnetization components aligned along the mixing axis or perpendicular to it, however with different efficiency. In cases where predominantly magnetization components aligned along one axis should be transferred spin-lock purge pulses (Section 2.3) with a duration of 1 to 2 ms are used before and after the mixing which dephase magnetization components not aligned with the mixing axis and remove partially contributions from anti-phase components. The two trim pulses must differ in their duration to prevent refocusing of unwanted signals. Alternatively phase cycled 90^o pulses of the form $90_{\phi 1}$-mixing-$90_{\phi 2}$ can be applied before and after the mixing sequence. For example, *y* magnetization can be selected to be mixed along the *y* axis using the four step phase cycle ϕ_1 = y, –y and ϕ_2 = y, y, –y, –y with constant receiver phase ϕ_r = x; when *y* magnetization should be mixed along the *z* axis the phase cycle ϕ_1 = x, –x and ϕ_2 = x, x, –x, –x with $\phi_r = \phi_1 + \phi_2$ can be used.

When applied to protons the TOCSY sequences in addition to the desired transfer due to scalar couplings exhibit an undesired transfer of magnetization *via* cross relaxation (ROE). The two pathways result in resonances with opposite signs so that they can in principle be distinguished. However in cases of overlapping resonances undesired cancellation effects may occur so that the elimination of the ROE contribution to [^{1}H, ^{1}H]-TOCSY spectra is desirable. Since transverse and longitudinal cross relaxation rates for proteins differ in their sign (Eq. (2.13) and Eq. (2.16)) a compensation scheme can be designed based on cancellation of the ROE by the NOE. The first scheme based on this idea used time periods during the mixing sequence where the magnetization stays aligned along the *z* axis [150]. The length of these time periods are adjusted for the NOE and ROE to cancel each other. Three different mixing schemes based on this scheme are in use: clean MLEV, DIPSI-2rc and clean CITY.

The MLEV-17 mixing scheme [44] was the first one modified for NOE/ROE compensation [150] (Table 7). The additional 17th pulse in MLEV-17 was added to the original MLEV-16 sequence [151] to compensate for phase and amplitude instabilities [44]. With modern NMR instruments the 17th pulse seems unnecessary and advantage can be taken from the somewhat larger bandwidth of MLEV-16. The mixing sequence MLEV-16 performs best for magnetization aligned along the spin-lock axis (y in Table 7). The more recently developed mixing sequence DIPSI-2rc [152] derives from the DIPSI sequence which has favourable magnetization transfer properties

but was optimized without including the delays for the ROE/NOE compensation. DIPSI-2rc is designed for coherence transfer starting with longitudinal magnetization (Table 7). The only sequence optimized including compensation delays is clean CITY [153]. This sequence offers a slightly larger bandwidth than clean MLEV-16 and a considerable larger bandwidth than DIPSI-

Table 7
Clean TOCSY mixing schemes

scheme	basic element R[†]	cycling of R[‡]	Δ[§]
clean MLEV-16	90_x-Δ-180_y-Δ-90_x	RR$\overline{\text{RR}}$ $\overline{\text{R}}$RR$\overline{\text{R}}$ $\overline{\text{RR}}$RR R$\overline{\text{RR}}$R	τ_{90}
DIPSI2-rc	180_x-Δ-140_x-320_{-x}-Δ-90_{-x}-270_x-Δ-20_x-200_{-x}-Δ-85_{-x}-30_x-125_{-x}-Δ-120_{-x}-300_x-Δ-75_x-225_{-x}-Δ-10_{-x}-190_x-Δ-180_x-Δ	R$\overline{\text{RR}}$R	τ_{144}
clean CITY	Δ-180_y-2Δ-180_y-Δ-48_{-x}-276_x-48_{-x}-Δ-180_y-2Δ-180_y-Δ	RR$\overline{\text{RR}}$	τ_{48}

[†] R is described by a series of *rf* pulses represented by their flip angles given in degrees and their phase indicated as a subscript, the pulses are separated by durations Δ.

[‡] Cycling scheme for the basic element R, $\overline{\text{R}}$ stands for the element R with all phases of the *rf* pulse changed by 180^o.

[§] The theoretical length of the compensation delay Δ in the limit for large molecules is indicated as the duration of a corresponding pulse in the sequence, for example τ_{144} stands for the duration of a 144^o pulse using the same power as for the mixing sequence.

2rc using the same average power. Clean CITY requires the magnetization entering the mixing scheme to be along the *z* axis (Table 7). All three mixing sequences contain time periods Δ during which the magnetization is longitudinal to compensate for the ROE. The theoretical values of Δ for the individual sequences listed in Table 7 are the lengths of a 90^o, a 144^o and a 48^o pulse, respectively. In practice Δ has to be adjusted to yield the best cancellation of ROE contributions and values about twice as large as the theoretical value are often obtained [150, 153].

There are mixing schemes available which do not use an explicit delay for the NOE compensation. The windowless sequence TOWNY [154] requires about 20% less peak power than MLEV-16. Another windowless sequence uses shaped pulses to reduce the average power required [155]. However these sequences may not suppress all ROE peaks and the compensation cannot be adjusted. In contrast, the sequences which use delays for the ROE/NOE compensation allow an easy adjustment to the specific experimental needs. In addition often the power applied for non-selective 90^o pulses in these pulse sequence can be used making power changes unnecessary. On the other hand sequences which compensate the ROE by delay periods for NOE do not mix isotropically, *i.e.* transverse magnetization components along the mixing axis and perpendicular to it as well as *z* magnetization are not transferred with the same efficiency. Homonuclear sensitivity enhancement [156] cannot be incorporated since this method requires isotropic mixing, such as provided for example by a DIPSI sequence (Table 8) without trim pulses before or after the mixing.

In practical implementations TOCSY sequences use an average field strength γB_1 which should be equal to 1.0 to 1.5 times the frequency range $\Delta\nu$ in which the spins should be efficiently mixed. Higher *rf* field strength could improve the performance of TOCSY mixing sequences, but heating effects in biological samples limit the power that can be applied. Whereas the average sample heating can be compensated by lowering the preset probe temperature (Section 3.5.3) the heating at some spots in the sample may be much larger than average. At such spots the temperature comes closer to the denaturation temperature of the proteins than expected from the average temperature increase. As a result protein molecules may aggregate and precipitate which not only causes a loss of protein but also disturbs the field homogeneity due the moving aggregates. The heating of the sample depends on the applied field strength and on the mixing time used. Typical mixing times for protons in proteins are in the range from 30 to 80 ms. The maximal mixing time is limited due to heating effects and relaxation. A good basis for the estimation of the required mixing time can be obtained from the time dependence of the coherence transfer by TOCSY mixing in homonuclear proton spin system [157].

When TOCSY sequences are applied to obtain coherence transfer in carbon spin systems ROE becomes negligible and windowless sequences are used. Efficient broadband isotropic mixing schemes must be used to cover the wider chemical shift range of carbon nuclei. The most commonly used sequences are DIPSI [158] and FLOPSY [159] (Table 8). The power that can be used for the mixing sequences is limited by the hardware and by the heating of the sample. Typically

Table 8
TOCSY mixing schemes

scheme	basic element R[†]	cycling of R[‡]
DIPSI-2	320_x-410_{-x}-290_x-285_{-x}-30_x-245_{-x}-375_x-265_{-x}-370_x	$R\overline{R}R\overline{R}$
DIPSI-3	245_{-x}-395_x-250_{-x}-275_x-30_{-x}-230_x-360_{-x}-245_x-370_{-x}-340_x-350_{-x}-260_x-270_{-x}-30_x-225_{-x}-365_x-255_{-x}-395_x	$R\overline{R}\overline{R}R$
FLOPSY-8	$46_0\ 96_{45}\ 164_{67.5}\ 159_{315}\ 130_{22.5}\ 159_{315}\ 164_{67.5}\ 96_{45}\ 46_0$	$R\overline{R}\overline{R}R\ R\overline{R}\overline{R}R$

[†] R is described by a series of *rf* pulses represented by their flip angles given in degrees and their phase x or –x indicated as a subscript, for FLOPSY *rf* phases are given in degrees.

[‡] Cycling scheme using the basic element R, $\overline{R}$ stands for the element R with all *rf* pulse phases changed by 180^o.

field strengths around 10 kHz are applied which can achieve efficient mixing between all aliphatic carbons when the offset is set in the middle of their resonance frequency range. Aromatic and carbonyl carbons in practice do not take part in this mixing but their resonances are disturbed by off-resonance effects. Whereas the DIPSI sequences are rather isotropic FLOPSY performs best when the mixing starts with magnetization along the *z* axis.

For an efficient TOCSY transfer in spin systems of coupled aliphatic carbons mixing times of 10 to 20 ms are usually employed. The field strength should be chosen as large as possible without substantial sample heating, but with a γB_1 not less than the frequency range to be covered. The length of the mixing time depends on the number of carbons to be correlated and the relaxation

rate of the carbons involved. The time dependence of homonuclear coherence transfer by ^{13}C isotropic mixing [160] can be used as a guideline to estimate the mixing time appropriate for the application.

4.2.2 Homonuclear through-space transfer

Through-space magnetization transfer can be obtained *via* cross relaxation in the laboratory frame (NOE) or the rotating frame (ROE). Transfer *via* NOEs is the basis of the homonuclear NOESY experiment [8, 9]. The NOESY segment consists of the mixing time τ_m which is flanked by two 90^o pulses (Fig. 15A). The first pulse of the NOESY segment transfers transverse magnetization components into I_z states which subsequently cross relax during τ_m with other protons in the protein (Section 2.1.6). In this way protons located within a distance of typically less than 0.5 nm can be detected. However, in the NOESY mixing time two additional transfer mechanisms may be present: chemical exchange and conformational exchange. Chemical exchange can for example be observed between water protons and amide protons located on the surface of a protein. In such experiments the water resonance must not be saturated before the NOESY mixing time (Section 5.3). Conformational exchange may occur in flexible parts of a protein, for example in loops connecting two secondary structure elements. When the two conformers exhibit different chemical shifts for a particular nucleus the NOESY segment will indicate a transfer of magnetization if the conformational exchange rate is of the order of the inverse mixing time. The three possible effects detected by NOESY cannot be distinguished without further information.

When coupled spins evolve into anti-phase states before the 90^o pulse that initiates the mixing time multiple quantum coherences may be created. Such states can be converted into undesired observable magnetization by the 90^o pulse that ends the mixing time and thus must be eliminated. Proper phase cycling or even more efficient, the application of a pulsed field gradient (PFG) during τ_m removes multiple quantum coherences with the exception of zero quantum coherence (ZQC). ZQC has coherence level 0, the same as the cross relaxing *z* magnetization and cannot be removed by PFGs or phase cycling. ZQC however does not give rise to a net transfer of magnetization so that the integrated intensities over the multiplet pattern is zero. This characteristic property permits in principle to distinguish NOE peaks from ZQC peaks. Still ZQCs may deteriorate

Fig. 15. Schemes for a homonuclear NOESY (A) and ROESY (B) transfer segment. For short mixing times τ_m (τ_m typically smaller 40 ms) the transfer from *S* magnetization to *I* magnetization, ΔI, is usually proportional to the *S* spin magnetization at the start of the mixing time, S^o (Eq. (2.12)): $\Delta I = \tau_m \sigma_N S^o$ for NOESY and $\Delta I = \tau_m \sigma_R S^o$ for ROESY.

the spectral quality since small NOEs may be severely distorted by overlap with ZQC resonances and an adequate integration of the NOE may no longer be possible. Thus the suppression of ZQCs is desirable. Unlike the I_z states ZQCs precess during the mixing time and this difference can be used to reduce the intensity of ZQC resonances. A slight variation of the mixing time τ_m

will not effect the NOE but will attribute a varying phase to the precessing ZQCs. Addition of individual scans with slightly differing τ_m will reduce their contribution to the detected signal [161]. A technique that randomly varies the mixing time within given limits cannot generally be recommended since the ZQC signals are smeared out and may give raise to increased t_1 noise in the spectrum [162]. Another simple scheme increments the initial mixing time τ_o by a constant small time interval $\Delta\tau_m$ in subsequent experiments. If *n* NOESY experiments are measured the ZQC can be substantially reduced in a certain bandwidth [163]:

$$\tau_m = \tau_o + n\Delta\tau_m \text{ with } \Delta\tau_m = (\Delta\nu_{min} + \Delta\nu_{max})^{-1} \tag{4.1}$$

where $\Delta\nu_{min}$ and $\Delta\nu_{max}$ are the minimal and maximal zero quantum frequencies that should be suppressed. The difference between τ_o and the maximal mixing time in the experiment should not exceed τ_o by more than 15%. About ten experiments with different mixing times according to Eq. (4.1) are measured and summed together with the contribution of the first and the last spectrum scaled down by a factor of two [163]. For special applications the frequencies of the ZQC in the indirect dimension can be shifted, however the shifted ZQC resonances may overlap with otherwise undistorted NOE peaks. A further interesting suppression technique removes zero quantum coherence with inhomogeneous adiabatic pulses [164] during the transfer from transverse to longitudinal magnetization. This method requires rather long transition periods of approximately 30 ms between fully transverse and cross relaxing *z* states, a time period which for many applications is prohibitively long.

The transfer segment based on ROE (Fig. 15B) consists of a spin-lock sequence with length τ_m during which cross relaxation in the rotating frame occurs. The sequence at first sight seems identical to a TOCSY sequence but for ROESY is suffices to apply only continuous wave (*cw*) *rf* irradiation at low power instead of the multipulse broadband inversion sequence necessary for TOCSY transfer. This results only in small interferences between ROESY and TOCSY which are much less severe than in the case of the TOCSY segment. A special suppression scheme is often not used since the bandwidth for TOCSY transfer with a low power *cw* spin-lock becomes very small. If still a better suppression is required techniques exist which reduce the residual TOCSY transfer in a ROESY sequence. The simplest method sets the offset for the ROESY spin-lock at one edge of the spectral range making the TOCSY transfer even more inefficient. Another approach applies a continuous frequency sweep to the carrier frequency of the spin-lock during its application [165] which strongly attenuates TOCSY contributions but hardly affects the ROE transfer. A third technique uses a special multipulse sequence for the suppression of TOCSY contributions [166], however the ROESY transfer with this scheme happens at a reduced rate which makes the sequence inefficient for most applications with proteins.

The *rf* field strength γB_1 used in ROESY corresponds to about one quarter of the frequency range $\Delta\nu$ which contains the signals of interest. Due to the low *rf* field strength used usually not more than 2.5 kHz, ROESY may suffer under off-resonance effects which cause varying transfer efficiency across the spectrum. The offset effects can be eliminated by two 90^o pulses which bracket the spin-lock mixing sequence [167]. This compensation introduces a phase distortion in the spectrum which is to a good approximation linear unless the frequency difference between two nuclei is much larger than the field strength γB_1 of the applied spin-lock field. An alternative scheme replaces the two 90^o by two 170^o pulses with just twice the power of the spin-lock which does not introduce a phase distortion but does not work well for offsets larger than the field strength applied [168]. The spatial inhomogeneity of the applied *rf* spin-lock field destroys all orders of multiple quantum coherences which may be present at the beginning of τ_m and only

zero quantum coherences will pass the mixing process. In the reference frame defined by the spin-lock field zero quantum coherence corresponds to anti-phase magnetization in the normal rotating frame or in the laboratory frame of reference. These signals can be suppressed using procedures corresponding to those applied in the NOESY sequence.

In applications with large molecules the mixing times in NOE and ROE experiments must be kept rather short otherwise the occurrence of spin diffusion (Section 2.1.6) will make the distance information obtained unreliable. The ROE sequence generates less spin diffusion artifacts than the NOE segment since the relayed magnetization has opposite sign and can be reduced by direct transfer [169]. For the NOE segment direct and relayed transfers have the same sign. To reduce spin diffusion contributions in selected frequency ranges in NOE spectra two techniques were developed. One technique uses the ROE effect to reduce contributions by spin diffusion [170, 171] and the other selective inversion of part of the resonances during the mixing time [172, 173].

ROE and NOE transfer provide very similar information based on different processes. The cross relaxation in the two mixing schemes, however, produces signals of different sign for large molecules (Eqs. (2.13) and (2.16)). On the other hand contributions from chemical and conformational exchange keep the same sign irrespective of the mixing scheme. Hence chemical and conformational exchange can be distinguished from cross relaxation in ROE spectra but not in NOE spectra. Based on this difference special experiments were developed which compensate NOE contributions by ROE and allow to detect chemical exchange free from interferences from cross relaxation [174].

4.2.3 Heteronuclear transfer

The efficiency of through-bond coherence transfer steps depends on the size of the coupling constants. Consequently using heteronuclear couplings is attractive because they are often much larger than proton-proton coupling constants (Fig. 5). The use of heteronuclear coupling constants, however, requires the protein to be labelled with ^{15}N and/or ^{13}C isotopes. In analogy to the homonuclear COSY segment, coherence transfer happens through anti-phase states (Fig. 16). For example, starting with heteronuclear anti-phase coherence prepared by an evolution segment (Fig. 12A) one 90^o pulse on *S* suffices to transfer anti-phase *I* spin coherence into two spin coherence (Fig. 16A, Table 9). A 90^o pulse on both the *I* and the *S* spins transfers anti-phase *I* spin coherence into an anti-phase *S* spin coherence (Fig. 16B, Table 9). Heteronuclear coherence transfer is the key segment in heteronuclear multidimensional experiments used with ^{15}N and/or ^{13}C labelled proteins.

A very important point to be considered in the context of coherence transfer schemes is the *S/N* obtainable from a particular experiment. The *S/N* depends on the polarization obtainable with the nuclei on which the pulse sequence starts and it depends on the size of the magnetization during detection of the signal. In other words the *S/N* depends on $\gamma_e B_o$ and on γ_d with the gyromagnetic ratios γ_e and γ_d of the excited and the detected nuclei, respectively (Table 1). Further the induced voltage is proportional to the resonance frequency $\omega_o = \gamma_d B_o$ of the detected nuclear species. On the other hand the noise contributed by the detection circuitry is proportional to the square root of the measured bandwidth. The necessary bandwidth increases linearly with ω_o and hence the noise is increased proportional to $\sqrt{\omega_o}$. Combining all this factors the *S/N* fulfils the following proportionality

Fig. 16. Schemes for heteronuclear polarization transfer starting from heteronuclear anti-phase magnetization. Narrow vertical bars stand for 90° *rf* pulses. The cartesian product operators indicated in the figure describe a typical coherence transfer step to heteronuclear multiple quantum (A) and to heteronuclear single quantum coherence (B). Transformation properties in the shift operator basis are given in Table 9.

Table 9
Heteronuclear through-bond transfer

Fig. 16	initial state	resulting product operators describing the transformation properties of the sequence†
A	$2I_zS_z$	$i(I_zS^+ - I_zS^-) = -2I_zS_y$
	$2I^+S_z$	$i(I^+ S^+ - I^+S^-) = -2I_xS_y - 2iI_yS_y$
	$2I^+S^+$	$(I^+S^- + I^+S^+) + 2iI^+S_z = 2I_xS_x - 2I_yS_z + 2iI_xS_z + 2iI_yS_x$
B	$2I_zS_z$	$(I^+ - I^-)\,(S^- - S^+)/2 = 2I_yS_y$
	$2I^+S_z$	$i(I^-+ I^+ + 2iI_z)\,(S^+ - S^-)/2 = -2I_xS_y - 2iI_zS_y$
	$2I^+S^+$	$(I^-+ I^+ + 2iI_z)(S^-+ S^+ +2iS_z)\,/2 = 2I_xS_x - 2I_zS_z + 2iI_xS_z + 2iI_zS_x$
† The resulting product operators are indicated in the shift and in the cartesian basis.		

$$S/N \propto \gamma_e \gamma_d^{3/2} B_o^{3/2} \qquad (4.2)$$

Eq. (4.2) demonstrates the benefits that can be obtained when the nuclei excited at the start of the pulse sequence and/or the nuclei detected are protons [175]. In addition Eq. (4.2) shows that coherence transfer steps to other nuclei between the excitation and detection do only influence the *S/N* through transfer efficiency and relaxation during the transfer.

The segment most frequently used to transfer magnetization from one nuclear species to another and to achieve the sensitivity improvement described by Eq. (4.2) is known under the acronym INEPT [45] which stands for "insensitive nuclei enhanced by polarization transfer". The INEPT scheme (Fig. 17A) combines the basic segments shown in Fig. 12A and Fig. 16B. By the way the discussion of the different representations used to describe NMR experiments (Fig. 3) is based on a INEPT type sequence. A full analysis of the INEPT scheme must include at least the spin systems *IS*, I_2S and I_3S which are of special interest since they represent the moieties $^{15}N^1H$, $^{13}C^1H$, $^{13}C^1H_2$ and $^{13}C^1H_3$ in labelled macromolecules. The much smaller homonuclear couplings are often neglected for the analysis of INEPT in terms of the product operator formalism (Table 10). The efficiency of the transfer depends on τ (Fig. 17A). A single value for τ exists for a simultane-

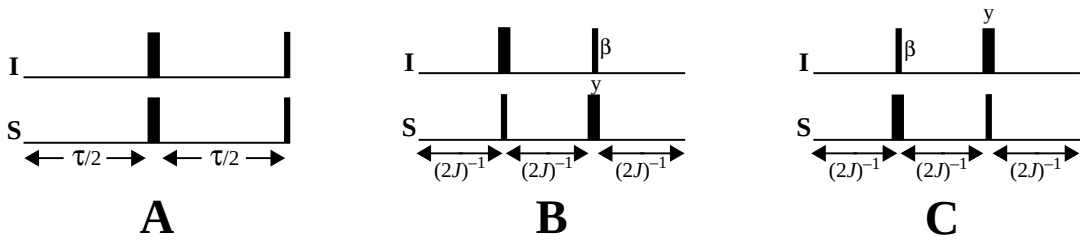

Fig. 17. Schemes for heteronuclear polarization transfer in I_nS spin systems. (A) INEPT segment using a heteronuclear single quantum coherence transfer step (HSQC). (B) and (C) DEPT segments where the pulse labelled β has varying flip angle β. (B) represents the coherence transfer from *I* to *S* spins and (C) from *S* to *I* spins. Table 10 presents the transformation properties of these segments. The contribution of the natural polarization of the destination spin can be subtracted from the measured signal by proper phase cycling (see text).

Table 10
INEPT and DEPT coherence transfer segments

Fig. 17	initial state	relevant product operators describing the transformation properties of the sequence†
A	I_x or I^+	$-2S_yI_z \sin(\pi J\tau) = \mathrm{i}(I_zS^+ - I_zS^-) \sin(\pi J\tau)$
	S_x or S^+	$-\sum_{k=1}^{n} 2I_{ky}S_z \cos^{n-1}(\pi J\tau) \sin(\pi J\tau) = \mathrm{i} \sum_{k=1}^{n} (I_k^+S_z - I_k^-S_z) \cos^{n-1}(\pi J\tau) \sin(\pi J\tau)$
B	I_x or I^+	$-S_x \cos^{n-1}\beta \sin\beta = \mathrm{i}(S^+ + S^-) \cos^{n-1}\beta \sin\beta /2$
C	S_x or S^+	$-\sum_{k=1}^{n} I_{kx} \cos^{n-1}\beta \sin\beta = -\sum_{k=1}^{n} (I_k^+ + I_k^-) \cos^{n-1}\beta \sin\beta /2$

† Only magnetization components transferred between *I* and *S* spins are shown. The natural magnetization of the destination spins is assumed to be subtracted from the resulting signal by proper phase cycling (see text). The expressions are valid for I_nS spin systems like the CH, CH_2 and CH_3 moieties in polypeptides. The scalar homonuclear coupling between the *I* spins is assumed to be much smaller than the heteronuclear coupling *J* between the *I* and *S* spins. The homonuclear couplings among the *I* spins are thus neglected in the product operator calculations. The resulting product operators are indicated in the shift and in the cartesian basis.

ous optimal transfer from *I* to *S* spins for all the three multiplicities *IS*, I_2S and I_3S. However, for the transfer from in-phase *S* magnetization to *I* magnetization τ depends on the multiplicity (Fig. 18). For a simultaneous transfer for all three multiplicities a value for τ of 0.33/*J* provides a good compromise.The different transfer functions allow editing of spectra according to the multiplicities of the resonance lines (Fig. 18). For example in a carbon spectrum the resonances of the CH, CH_2 and CH_3 groups can be separated into different spectra [16, 24, 26].

For best performance INEPT requires the coupling constants used to prepare the coherence transfer step to have the same value, a condition often fulfilled for spin systems in proteins. For cases with sizeable variations of the heteronuclear coupling constants used for the polarization transfer

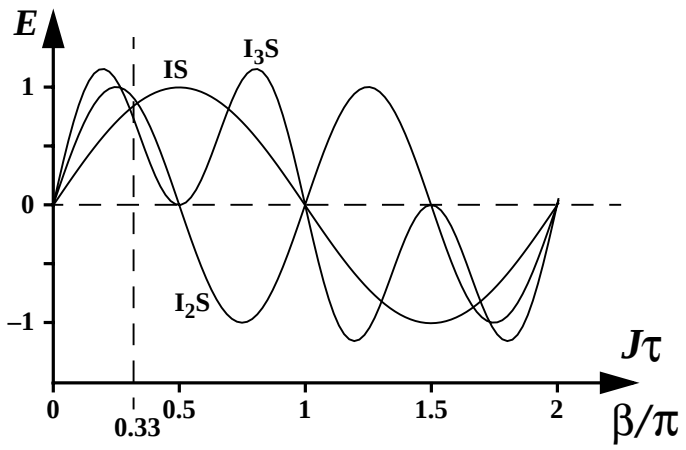

Fig. 18. Coherence transfer efficiency E for heteronuclear polarization transfer in the spin system IS, I_2S and I_3S versus $J\tau$ for the INEPT or β/π for the DEPT segment. J is the scalar coupling constant between the nuclei I and S, τ the period during which the state evolves due to the coupling J and β is the flip angle of the pulse with variable length in the DEPT sequence (Fig. 17). The value 0.33 for $J\tau$ or β/π indicates a compromise value often used when simultaneous in-phase magnetization transfer to or from carbon nuclei in CH, CH_2 and CH_3 moieties is required.

an alternative polarization transfer scheme, DEPT [176], offers superior performance at the cost of a longer sequence. DEPT stands for distortionless enhancement by polarization transfer. In contrast to INEPT the DEPT sequence achieves spectral editing on the basis of spectra measured with different flip angles for the pulse β in the sequence (Fig. 17B, Table 10) and not by changing a delay period. The complete DEPT segments in Fig. 17B and C transfer in-phase magnetization into in-phase magnetization. This is in contrast to the INEPT segment shown in Fig. 17A where the sequence starts with in-phase magnetization and ends with transferred magnetization in anti-phase which must first be refocused by the segment shown in Fig. 12A with the refocusing delay optimized according to Fig. 18. For heteronuclear polarization transfer in proteins the INEPT segment is used much more frequently than DEPT since the coupling constants used are fairly homogeneous, the possible distortions are less disturbing for large linewidths, and quite often the faster transfer into anti-phase states is preferred to minimize relaxation losses. In addition, even for an in-phase magnetization transfer the duration of an INEPT based sequence is shorter than DEPT.

Multidimensional NMR experiments often contain several INEPT steps. For the implementation of consecutive INEPT segments two different methods exist: "out-and-back" and "out-and-stay" (or "straight-through") experiments. The first type retains anti-phase magnetization to the nucleus where the magnetization originates. A further INEPT step brings the magnetization back to the original nucleus. In an "out-and-stay" transfer the anti-phase magnetization obtained after the transfer is refocused on the destination nucleus and finally measured on a nucleus different from the one on which the polarization transfer started. Experiments using the "out-and-back" technique often offer a better sensitivity than "out-and-stay" experiments since the relaxation of transverse magnetization on fast relaxing nuclei can be minimized due to the shorter transfer times.

In practical implementations of the polarization transfer sequences discussed a few points

deserve consideration. When transferring magnetization from *I* spins to *S* spins often the natural *S* spin polarization interferes with the measurement and must be removed, for example, by applying the two step phase cycle (x, –x) to one of the 90^o pulses applied to the *I* spins before the transfer and subtracting the signals thus obtained. In the DEPT segment often the phase of the pulse β is cycled using this scheme. Further, to make sure that the magnetization detected was transferred through the desired heteronucleus *S*, the 90^o *S* pulse accomplishing the polarization transfer is cycled in the same way. For optimal polarization transfer the length of the period to obtain anti-phase magnetization is often chosen shorter than dictated by the *J* coupling involved to counteract relaxation. When a polarization transfer step immediately follows an evolution time only half of the magnetization, either the sine or the cosine component created due to chemical shift evolution, can be transferred. However in some cases the application of a sensitivity enhancement scheme using a heteronuclear multiple quantum state retains both components [177] (Section 4.5.3). The best enhancement is achieved for two spin systems like the $^{15}N^{1}H$ moiety.

In analogy to TOCSY transfer in homonuclear spin systems the heteronuclear *J* cross polarization experiment [178] (Fig. 19) presents an alternative to coherence transfer *via* anti-phase states. Three major differences distinguish heteronuclear Hartmann-Hahn (HEHAHA) experiments from homonuclear TOCSY: for HEHAHA the *rf* fields applied at different frequencies must match the condition given in Eq. (2.10), the heteronuclear transfer is a factor two slower (Eq.

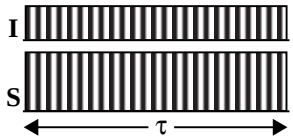

Fig. 19. Pulse sequence segment used to obtain heteronuclear Hartmann-Hahn polarization transfer. The hatched rectangles indicate continuous application of *rf* pulses. The strengths of the two different *rf* fields applied to the *I* and *S* spins must fulfil the Hartmann-Hahn condition given in Eq. (2.10). The magnetization transfer obtained for a heteronuclear two-spin system is described in Eq. (2.11).

(2.9) and Eq. (2.11)) and heteronuclear ROESY contributions can be neglected. Complete magnetization transfer from the *I* spins to the *S* spins in a heteronuclear two spin system requires the same amount of time as the in-phase transfer *via* an INEPT scheme. A full transfer into anti-phase magnetization cannot be obtained (Eq. (2.11)). Therefore, heteronuclear *J* cross polarization presents mainly an alternative for the "out-and-stay" type of experiments whereas for the more frequently used "out-and-back" experiments the INEPT sequence is usually more efficient. HEHAHA experiments can have an advantage over INEPT when simultaneous homonuclear and heteronuclear coherence transfers are desired. Investigations on double and triple HEHAHA experiments in comparison to INEPT type experiments show however only a small overall advantage of the cross polarization method [179].

When implementing HEHAHA sequences the Hartmann-Hahn condition must be fulfilled (Eq (2.10). The best matching can be obtained when the frequencies for the nuclei are delivered from the same *rf* coil since then the *rf* homogeneities of the two fields are the same. HEHAHA sequences contribute to the heating of the sample and of the probe circuitry which may detune the coil and, hence, affect the Hartmann-Hahn transfer efficiency. Historically multipulse broadband decoupling sequences were used for heteronuclear cross polarization but the conditions for

broadband cross polarization are more restrictive than those for decoupling and the best sequences for the former will be efficient for the latter but not vice versa. The most frequently used HEHAHA mixing sequences are DIPSI-2 and DIPSI-3 [158] (Table 8), but alternative sequences have been proposed [180, 181]. HEHAHA experiments can also be applied band selectively using trains of shaped pulses [182].

4.3 Decoupling sequences

The scalar coupling between nuclei finds frequent application for the manipulation of spin states or for the determination of dihedral angles [42]. On the other hand couplings may complicate spectra and reduce the maximal signal intensity. If only the spin state at the end of a time period τ is of interest the evolution due to J coupling between two nuclei can be refocused by a 180^o pulse applied to one nucleus in the middle of τ (Section 4.1). Fig. 20A shows a more general case where I_k and H_k represent spins from the same species whereas S_k stands for spins from a different species. The spins I_k are decoupled from the S_k spins by a 180^o pulse on the S_k spins. At the same time a frequency selective 180^o inversion pulse applied to the H_k spins decouples the I_k spins from the H_k spins. Fig. 20B presents a very special decoupling sequence that decouples two spins of the same nuclear species but still maintains the evolution due to their chemical shifts [183]. Starting with y magnetization the analysis of this sequence with the product operator formalism shows that at the end of a time period $2t$ the evolution due to J coupling is refocused and that both spins have evolved due to their chemical shifts for a time period t.

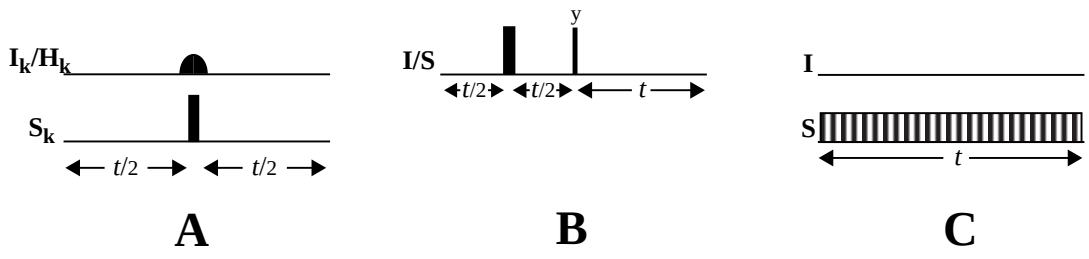

Fig. 20. Decoupling schemes. (A) Transverse magnetization of the spins I_k is decoupled from the S_k spins by a 180^o pulse applied to the S_k spins. At the same time a frequency selective 180^o inversion pulse on the H_k spins which are of the same species as the I_k spins decouples the I_k spins from the H_k spins. (B) Special scheme for a homonuclear two spin system that decouples the two spins I and S from each other and still maintains chemical shift evolution of both spins during a period t. The initial state $I_y + S_y$ is transformed to $-I_x\sin(\omega t)+I_y\cos(\omega t)-S_x\sin(\Omega t)+S_y.\cos(\Omega t)$ at the end of the sequence. (C) The I spins are decoupled from the S spins by a broadband composite pulse decoupling sequence (Table 11).

If decoupling must be maintained over extended time periods, for instance during the acquisition of the signal, continuous multipulse sequences are applied (Fig. 20C). Much effort has been expended to develop heteronuclear decoupling sequences that increase the effective decoupling bandwidth without increasing the *rf* power dissipation in the sample while keeping the residual splitting much smaller than the linewidth of the resonances observed. The first heteronuclear broadband decoupling technique to appear in the literature applied noise irradiation at the frequency of the undesired coupling partner [184]. Since then heteronuclear broadband decoupling techniques have improved enormously, initially through various forms of composite pulse decou-

pling [151, 158, 185, 186] and more recently using methods based on adiabatic fast passage [187–191]. Despite their increased efficiency decoupling sequences very likely increase the average sample temperature, this effect should be compensated by lowering the preset temperature (Section 3.5.3). Decoupling sequences applied during non-constant time periods *t* in multidimensional experiments may result in increasing average sample temperatures with increasing values of *t* which will cause severe distortions in the spectrum. A constant sample temperature over the whole experiment can be obtained by decreasing a continuous wave irradiation after acquisition concomitant with the increasing time period *t* [192].

The most frequently used decoupling schemes are WALTZ [185], GARP [186], DIPSI [158] and more recently adiabatic schemes such as WURST [191]. A measure of the efficiency of a particular decoupling scheme is given by the frequency range decoupled by a certain average field strength. For example a *rf* field of 4 kHz decouples a frequency range of 1.2 kHz with noise decoupling, 7.2 kHz with WALTZ-16, 19 kHz with GARP-1 and 78 kHz with WURST decoupling [193]. Multipulse decoupling sequences consist of a basic element R which is repetitively applied in combination with the element $\overline{R}$. In the element $\overline{R}$ all the phases of the *rf* pulse are shifted by 180^o for the improvement of the decoupling performance [151]. In Table 11 composite pulse decoupling sequences are represented by their basic segment R given by a train of *rf* pulses which are indicated by their flip angles in degrees. The pulses are applied with phase x or –x which are indicated as a subscript.

Table 11
Composite pulse decoupling schemes

scheme	basic element R†	cycling of R‡	$\Delta\nu$§	length of R*f*
Waltz-16	90_x-180_{-x}-270_x	$R\overline{R}\overline{R}R$ $\overline{R}R\overline{R}R$ $\overline{R}\overline{R}RR$ $R\overline{R}\overline{R}R$	±1.0	540
GARP-1	30.5_x-55.2_{-x}-257.8_x-268.3_{-x}-69.3_x-62.2_{-x}-85.0_x-91.8_{-x}-134.5_x-256.1_{-x}-66.4_x-45.9_{-x}-25.2_x-72.7_{-x}-119.5_x-138.2_{-x}-258.4_x-64.9_{-x}-70.9_x-77.2_{-x}-98.2_x-133.6_{-x}-255.9_x-65.5_{-x}-53.4_x	$R\overline{R}\overline{R}R$	±2.4	2857
DIPSI-2	320_x-410_{-x}-290_x-285_{-x}-30_x-245_{-x}-375_x-265_{-x}-370_x	$R\overline{R}\overline{R}R$	±0.6	2590
DIPSI-3	245_{-x}-395_x-250_{-x}-275_x-30_{-x}-230_x-360_{-x}-245_x-370_{-x}-340_x-350_{-x}-260_x-270_{-x}-30_x-225_{-x}-365_x-255_{-x}-395_x	$R\overline{R}\overline{R}R$	±0.8	4890

† R is described by a series of *rf* pulses represented by their flip angles given in degrees and their phase x or –x indicated as a subscript.

‡ Cycling scheme for the basic element R; $\overline{R}$ stands for the element R with all phases of the *rf* pulse changed by 180^o.

§ Decoupled bandwidth $\Delta\nu$ given in units γB_1 of the applied *rf* field strength.

f Total length of the element R given as a pulse angle in degrees.

The modern repetitive heteronuclear decoupling schemes in general are susceptible to the prob-

lem of cycling sidebands. Viewed in the time domain, decoupling consists basically of a repeated refocusing of the divergence of magnetization vectors due to the spin-spin coupling. Unless the focusing is precise and the sampling of the observed signal is exactly synchronized with the focus points, decoupling introduces spurious modulations into the free induction decay. The Fourier transform of these oscillatory artifacts consists of pairs of modulation sidebands flanking the resonance frequency and separated from it by the cycling frequency. These cycling sidebands may severely distort the quality of spectra with largely different peak intensities such as NOESY spectra [194]. Cycling sidebands can be minimized using high decoupling power, but this conflicts with the goal of achieving the desired decoupling bandwidth with lowest possible sample heating. Different techniques to reduce sideband intensities have been developed [195, 196] but depending on the application only certain techniques may give sufficient reduction. An almost complete suppression can be obtained even at low decoupling power using a WURST decoupling scheme, ECO-WURST [194], with two different decoupling powers which are applied for a variable length of time in different scans. The ECO-WURST scheme permits, for example, the detection of weak cross peaks close to strong direct correlation peaks in multidimensional heteronuclear decoupled ^{1}H-detected NMR experiments.

In contrast to conventional composite pulse decoupling schemes (Table 11) efficient adiabatic decoupling schemes cover chemical shift ranges that far exceed those required for ^{13}C on a 800 MHz spectrometer [193]. However adiabatic decoupling schemes may have considerable sideband intensities which are even more obstructive when the adiabatic condition is not properly fulfilled and when the pulse repetition rate is insufficiently high in comparison with the coupling constant. The sweep rate is therefore a compromise between two requirements: it must be slow enough to satisfy the adiabatic condition given in Eq. (2.26) and fast enough so that the product of the coupling constant J and the sweep duration is approximately 0.2. A guide to optimize the decoupling performance by choosing the most suitable instrumental settings has been published for WURST decoupling [193]. As an example, WURST decoupling with an average *rf* field strength of 4 kHz using a frequency sweep over 70 kHz with a rate of 145 MHz/sec decouples a bandwidth of 30 kHz with minimal sidebands if the coupling constant does not exceed 150 Hz.

One important criterion for the selection of decoupling sequences is the requirement to limit the heating of the sample and thus often the widest bandwidth per unit power is favoured. GARP and schemes based on adiabatic pulses offer wide decoupling bandwidth but also suffer from considerable cycling sideband intensities. At the cost of a smaller decoupling bandwidth WALTZ provides smaller sidebands and very small residual splittings of the decoupled resonances. The latter feature is less important in protein spectra with their inherently broad lines. In systems requiring relatively small decoupling bandwidths which have homonuclear couplings among the decoupled spins DIPSI sequences may outperform WALTZ and GARP especially at low power levels [158]. DIPSI was optimized including the effect of spin-spin coupling among the spins irradiated.

Not only are multipulse decoupling sequences used for heteronuclear decoupling but they find application as narrow band homonuclear decoupling schemes. The primary goal in these applications is to decouple a narrow range of frequencies with minimal disturbance outside of this region. Examples are the decoupling of amide protons resonances from α protons or the decoupling of aliphatic carbon resonances from carbonyl carbons. For homonuclear bandselective decoupling three different techniques are used. In the first method the high power 180^{o} pulses employed in evolution schemes for decoupling purposes can be replaced by selective pulses with a box like inversion profile resulting in a bandselective decoupling (Fig. 20A). The same class of pulses can also be applied to obtain homonuclear decoupling during the acquisition of the signal

[197], but this requires interleaved acquisition (Section 2.4.3). A second method uses composite pulse decoupling schemes replacing the high power rectangular pulses normally used with low power shaped pulses thus obtaining a composite pulse decoupling sequence with narrow bandwidth [198–200]. A third method adapts adiabatic decoupling schemes for narrowband homonuclear decoupling [201]. All homonuclear decoupling sequences may cause phase and frequency shifts for the resonances outside the irradiated bandwidth by non-resonant effects which are summarized in Eqs. (2.21) to (2.23).

4.4 Pulsed magnetic field gradients

The use of pulsed magnetic field gradients (PFGs) in high resolution NMR has become a routine technique in the last few years [71, 72]. This breakthrough is due to the availability of shielded gradient coils which improve the performance of PFGs dramatically. Older gradient coil designs generated eddy currents which compromised field homogeneity and required unacceptable periods to decay. Shielded gradients do generate much smaller eddy currents resulting in substantially reduced recovery times. PFGs perform a variety of functions in pulse sequences. They can be used for reduction of phase cycling which saves measurement time for sufficiently concentrated samples, for elimination of experimental artifacts, for suppression of t_1 noise, for suppression of strong solvent lines and for measuring diffusion properties. Gradients up to 0.3 T/m (30 G/cm) are usually sufficient for most of these applications. Much stronger gradients can distort the NMR spectrum unless special techniques [68] and/or long recovery times are used after the application of a PFG. The applications of PFGs can be grouped into three different categories which are briefly discussed in the following: use of spatial frequency dependence, destruction of coherences and selection of coherences.

During the application of a PFG the resonance frequency of a nucleus depends on its spatial location (Eq. 2.30). The signal defocused by a PFG cannot completely be refocused by a second gradient if the molecules have diffused to another location between the two gradients. This effect finds direct application in diffusion measurements, but of course, is always present when gradients are used. This can lead to accidental signal loss when defocusing and refocusing gradients are separated by a long time period. Fig. 21 shows a typical sequence used for measuring diffusion constants. Translational diffusion in liquids during a time interval T results in different NMR

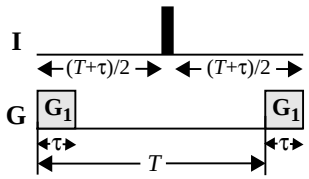

Fig. 21. Gradient scheme for diffusion measurements. A series of experiments is performed with different gradient strength G_1 keeping the time period T constant to exclude interferences from relaxation processes. With increasing values for G_1 the signal intensities obtained decay exponentially according to Eq. (4.3).

signal intensities depending on whether or not T is bounded by two identical PFGs with strength

G_1 (Fig. 21). The signal intensities S with and S_o without gradients fulfil the relation [67]

$$\ln(S/S_o) = -\gamma^2\tau^2 G_1^2(T - \tau/3)D \qquad (4.3)$$

where D is the translational diffusion coefficient, γ the gyromagnetic ratio (Table 1), τ the length of the gradient, and T the time period between the start of the two gradients (Fig. 21). Depending on the solvent conditions water molecules diffuse about 10 to 50 times faster than proteins in the molecular weight range from 5 to 25 kDa. For example, the self-diffusion constants of water molecules and of the protein BPTI in a highly concentrated 20 mM BPTI solution in 90%H_2O/ 10%D_2O at 4°C are $1.0 \cdot 10^{-9}$ m^2/s and $4.7 \cdot 10^{-11}$ m^2/s, respectively [68, 202]. Diffusion weighting of the NMR signal can be used to separate resonances of large and small molecules [202, 203]. In another application diffusion constants measured with NMR are used to characterize the aggregation state of proteins [204, 205].

Very frequently PFGs are used to destroy unwanted transverse magnetization where the magnetization of interest is in a z state. If sufficient time is allowed after the gradient for the field homogeneity to recover the implementation is simple and only accidental refocusing of unwanted magnetization must be prevented. This application does not require special linearity and reproducibility of the gradients. Fig. 22 presents typical pulse sequence segments used to destroy

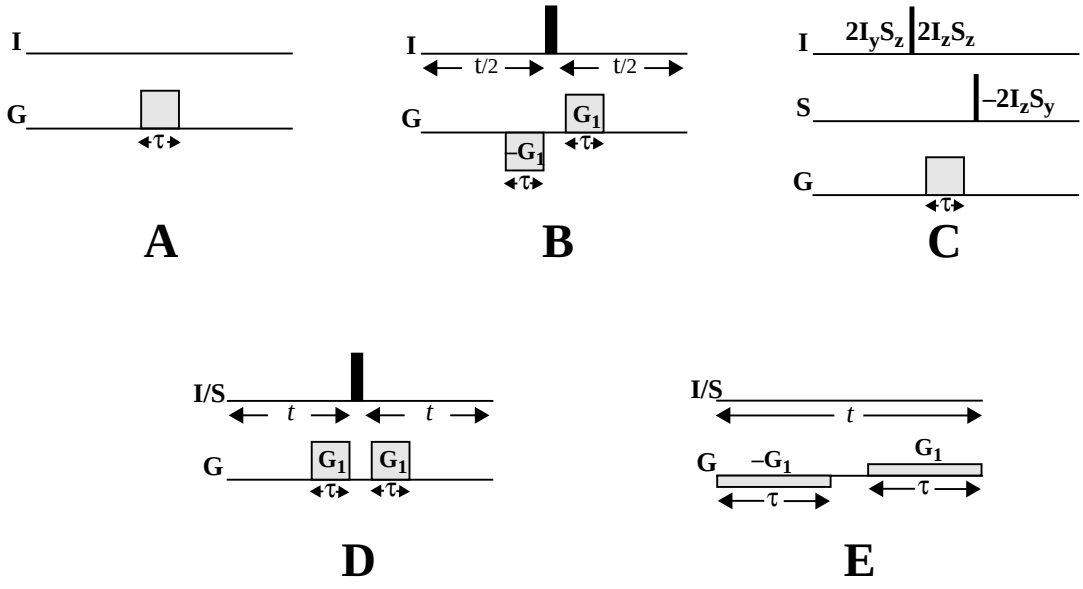

Fig. 22. Gradient schemes that destroy unwanted signals. (A) All magnetization components are destroyed except for z magnetization, z ordered states and zero quantum coherences. (B) This sequence destroys the same states as (A) and in addition all magnetization components created by a non-ideal 180° inversion pulse on z states. (C) Scheme frequently used to destroy unwanted magnetization components in a heteronuclear polarization transfer step, the desired magnetization is in a z ordered state during the gradient. The cartesian product operators indicate typical states which can survive the PFG. (D) Selection of all magnetization components that are properly inverted or refocused by the 180° pulse. (D) The scheme uses very weak gradients and leaves all magnetization components practically unchanged but prevents radiation damping of strong solvent resonances.

undesired magnetization components. The segment in Fig. 22A destroys all transverse magneti-

zation except zero quantum coherence. The segment in Fig. 22B acts like the one in Fig. 22A and in addition destroys all magnetization components originating from *z* states which are not properly inverted by the 180° pulse. Fig. 22C presents a very popular application in heteronuclear coherence transfer steps where the magnetization of interest is in a *z* ordered state during the application of the gradient. In this context it is worth noting that for example two spin order, I_zS_z, can relax substantially faster than for example S_z magnetization due to additional contributions to relaxation from proton-proton dipolar interactions [206]. For this reason gradient and recovery delay should be kept sufficiently short to prevent relaxation losses. Fig. 22D and E show segments which not only destroy undesired magnetization but at the same time retain desired transverse magnetization. This requires exactly reproducible gradients which refocus the magnetization of interest. Fig. 22D shows an efficient alternative to phase cycles such as EXORCYCLE (Section 2.2.1). This segment retains only transverse and longitudinal magnetization components that are properly inverted or refocused by the 180° pulse. The segment in Fig. 22E restores all magnetization at the end of the time period *t* and leaves ideally all magnetization components unchanged. Using weak gradients the segment prevents only radiation damping of very intense solvent resonances [90].

The third category of applications of PFGs, coherence selection, requires linear gradient amplifiers and precisely reproducible gradients where the absolute strength for positive and negative gradients match exactly. Otherwise tedious optimization procedures are necessary to obtain the maximal signal. Fig. 23 presents typical applications of PFGs for coherence selection and Table 12 summarizes the characterization of these segments using the product operator formalism.The segment shown in Fig. 23A demonstrates the selection of a transfer from a double quantum to a single quantum state by PFGs [207]. Double quantum coherence before the 90° pulse is defocused by a gradient as described by Eq. (2.30). Refocusing the magnetization in a single quantum state requires a PFG with the product $G_2\delta$ of the strength G_2 and duration δ of the gradient to be double compared to the first PFG (Fig. 23A). The segment in Fig. 23B uses the same principle for the selection of anti-phase magnetization during a heteronuclear coherence transfer step. A PFG is applied to anti-phase magnetization of spin *I*. After the coherence transfer step to anti-phase *S* spin magnetization a second PFG with the appropriate product $G_2\delta$ must be applied to refocus the desired magnetization. The spread of resonance frequencies introduced during a PFG depends on the gyromagnetic ratio γ (Eq. 2.30)) and hence the condition $G_2\delta = \gamma_I G_1\tau/\gamma_S$ must be fulfilled for the segment in Fig. 23B. In a more general case the sum of all the exponential factors described by Eq. (2.30) which are introduced by gradients during the pulse sequence must vanish to result in observable magnetization [71, 72].

The application of PFGs for the selection of coherence pathways cannot retain positive and negative coherence levels simultaneously (Eq. (2.30)) which results in a loss of half of the signal. Thus one coherence selection step using gradients reduces the obtainable *S/N* by $\sqrt{2}$ compared to the selection by a phase cycling scheme. When applying a PFG for coherence selection during an evolution time of a multidimensional experiment the requirement to retain both coherence levels cannot be fulfilled and pure phase absorptive spectra cannot be obtained (Section 2.5). Pathways for both positive and negative coherence levels can only be obtained using a second scan with the inversion of the sign of one of the gradients used for the selection. In some experimental schemes part of the detectable magnetization can be destroyed to obtain pure phase spectra, but such a procedure reduces the sensitivity even more [208]. On the other hand enhancement schemes exist for gradient selected coherence pathways (Section 4.5.3).

In practical implementations very long and/or very strong PFGs may still require long

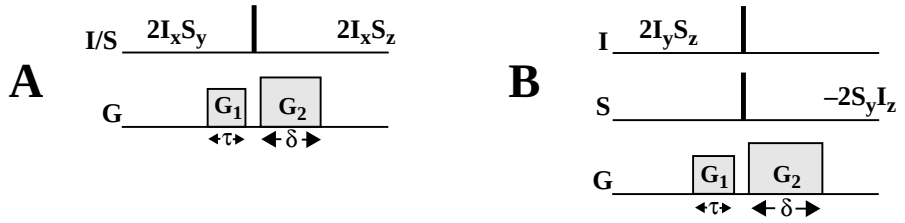

Fig. 23. Examples of schemes that select the desired signal by the application of PFGs. The transformation properties for I^+ states are given in Table 12. (A) Selection of a homonuclear coherence transfer pathway from a two quantum to a single quantum state. The product between the strength of the gradient and its duration must fulfil the equation $G_2\delta = 2G_1\tau$. (B) Selection of a heteronuclear coherence transfer step where $G_2\delta = \gamma_I G_1\tau/\gamma_S$. The cartesian product operators indicated in (A) and (B) describe a typical coherence transfer step selected by the PFGs.

Table 12
Coherence selection by PFGs

Fig. 23	initial state	resulting product operators describing the transformation properties of the sequence†
A	I^+	0
	$2I^+S_z$	0
	$2I^+S^+$	$iS^-I_z\, e^{-i(\omega + \Omega)\tau+i\omega\delta} + iI^-S_z\, e^{-i(\omega + \Omega)\tau+i\Omega\delta}$
B	I^+	0
	$2I^+S_z$	$S^-I_z\, e^{-i\omega\tau\, +ik\Omega\delta}$ with $k = \gamma_I/\gamma_S$
	$2I^+S^+$	0

† The coherence selection is described from the start of the first to the end of the second PFG neglecting scalar couplings.

recovery times compared to the relaxation of transverse magnetization and may cause signal loss. In such situations a preemphasis unit may be useful to reduce recovery times. This unit shapes the gradient pulses, for example using exponential functions with different time constants and amplitudes. The preemphasis unit compensates the transient response induced in the system when switching on or off magnetic field gradients resulting in shorter recovery times. The adjustment requires manipulations which are similar to shimming a magnet and may require substantial time and experience. The complex spatial and time dependencies of the induced transient effects often exclude their complete compensation. When working with triple axis gradients a preemphasis may be desirable even for moderate gradient strengths because the different gradient coils can exhibit interactions resulting in longer recovery times compared to a single axis gradient system.

4.5 Combinations of basic segments

4.5.1 The HSQC and the HMQC scheme

The heteronuclear single quantum coherence (HSQC) transfer and the heteronuclear multiple quantum coherence (HMQC) transfer are the two most frequently used schemes for coherence transfer in heteronuclear multidimensional NMR experiments. Both schemes include two coherence transfer steps separated by an evolution period t_1 to sample the resonance frequencies of one nuclear species (Fig. 24). The HSQC consists of two INEPT steps (Fig. 17A) leading to heteronuclear single quantum coherences during t_1 whereas the coherence transfer steps (Fig. 16A) used in HMQC create multiple quantum coherences which evolve during t_1. At least two coherence transfer steps are required in heteronuclear coherence transfer experiments since best sensitivity can usually be obtained if the nucleus with the highest gyromagnetic ratio is excited and detected (Eq. (4.2)).

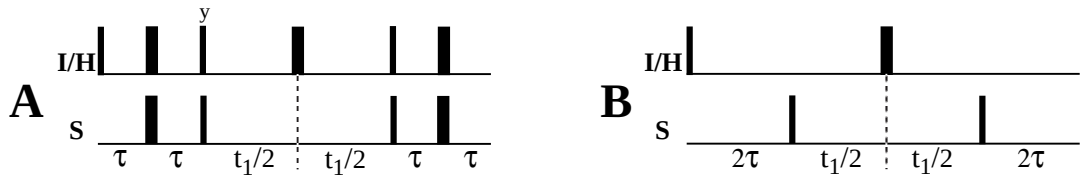

Fig. 24. Coherence transfer schemes transferring heteronuclear single quantum coherence (A) and heteronuclear multiple quantum coherence (B) which are often referred to as HSQC and HMQC schemes, respectively. The time period τ is set to $(4J)^{-1}$ or slightly shorter to compensate for relaxation losses. These sequences can easily be described using the product operator formalism. Table 13 presents the resulting operators at the end of the sequence for a three spin system with two scalar coupled spins *I* and *H* of the same species and one spin *S* of a different species scalar coupled only to *I* spins.

Table 13
Coherence transfer by HSQC and HMQC schemes

Fig. 24	initial state	resulting product operators describing the transformation properties of the sequence†
A	I_z	$I_x \cos(\Omega t_1) \cos^2(2\pi J_{II}\tau) \sin^2(2\pi J\tau) + I_y H_z \cos(\Omega t_1) \sin(4\pi J_{II}\tau)\sin^2(2\pi J\tau)$
B	I_z	$I_y \cos(\pi J_{II}(t_1 + 4\tau))\,(\cos^2(2\pi J\tau) - \cos(\Omega t_1) \sin^2(2\pi J\tau))$ $+ 2I_x H_z\, sin(\pi J_{II}(t_1 + 4\tau))\,(\cos(\Omega t_1) \sin^2(2\pi J\tau) - \cos^2(2\pi J\tau))$

† A three spin system is considered with two spins, *I* and *H*, belonging to the same nuclear species and one spin *S* of a different species. Spin *S* is scalar coupled only to *I* and not to *H*. The heteronuclear coupling constant is denoted *J* and the homonuclear coupling between *I* and *H*, J_{II}. Only operators that lead to detectable in-phase magnetization with respect to spin *S* are shown. Signals originating from polarizations of *H* and *S* spins at the beginning of the sequence are assumed to be cancelled by an appropriate phase cycling scheme.

The two schemes differ in important features [209]. Because the HMQC has a much smaller number of rf pulses it is less prone to pulse imperfections. In addition, multiple quantum coherences may have better relaxation properties than corresponding single quantum states, an advantage that can be exploited by using a HMQC transfer. The improved relaxation properties are explained by the different dependence on the spectral density at zero frequency $J(0)$ (Section 2.1.4). When a HMQC sequence is applied to a two spin system zero quantum (ZQC) and double quantum coherences (DQC) exist during the evolution period. The transverse relaxation for ZQC and DQC based on dipolar interactions does not depend on $J(0)$ [16, 29], in contrast to the single quantum coherence present in the INEPT sequence where the dependence on $J(0)$ contributes a major part to the relaxation. However, when more than two spins are considered the multiple quantum states can loose the relaxation advantage due to dipolar interactions with additional protons [210]. Further, the HMQC scheme may not be optimal to obtain good resolution in the indirect dimension because the homonuclear couplings, J_{II}, among the *I* spins modulate the signal of the *S* nuclei which broadens the resonance lines in the spectrum. In the HSQC these couplings are not active during the evolution time (Table 13). The description of the two sequences in the product operator formalism given in Table 13 demonstrates that the homonuclear couplings J_{II} reduces the signal slightly for the HSQC whereas a phase shift $4\pi J_{II}\tau$ is introduced into the indirect dimension of the HMQC experiment which cannot be corrected since J_{II} varies randomly from resonance to resonance. In addition the homonuclear coupling among the *I* spins leads to a contribution of homonuclear anti-phase dispersive signals. These signals usually do not disturb spectra of proteins due to the inherently broad linewidths.

In both schemes shown in Fig. 24 the *S* spins evolve not only due to the chemical shift but also due to their homonuclear couplings J_{SS} introducing line splittings in well resolved spectra. Often only the heteronuclear correlations between the *I* and *S* spins are of interest whereas the resolved couplings are undesired. This requires a scheme during which the spins evolve due to chemical shifts but not due to homonuclear couplings. Fig. 25 presents a sequence that fulfils these boundary conditions [211, 212]. The segment has a fixed duration 2*T*. The evolution of the *S* spins due to homo- and heteronuclear scalar couplings does not depend on the chemical shift evolution time *t* which can be changed in the range from 0 to 2*T*. In this constant-time (*ct*) evolution segment (Fig. 25) the modulation of the signal due to its chemical shift is obtained by moving the two 180^o pulses as indicated in Fig. 25. The two 180^o pulses have a fixed separation of length *T*

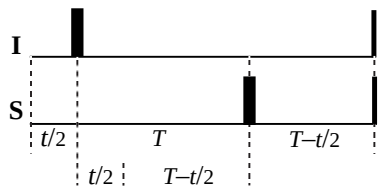

Fig. 25. Constant time (*ct*) chemical shift evolution period with a fixed duration 2*T*. The separation of the two 180^o *rf* pulses stays constant at *T*. For all values of *T* the evolution of the *S* spins due to scalar coupling to the *I* spins is refocused. If 2*T* is set to a multiple of $1/J_{SS}$, where J_{SS} is the coupling between the *S* spins, homonuclear decoupling of the *S* spins can be obtained. The maximal evolution time for the *S* spins due to their chemical shift is 2*T*.

and the delay t is incremented according to the frequency range desired in the spectrum (Table 3). If the homonuclear couplings J_{SS} among the S spins have a narrow range of values the time period $2T$ can be set to a multiple of $1/J_{SS}$ to obtain a homonuclear decoupled spectrum of the S spins. For example, the aliphatic carbon spin systems in fully ^{13}C labelled proteins have coupling constants in a narrow range around 35 Hz except for the coupling to the carbonyl carbons which can easily be decoupled by conventional decoupling (Section 4.3). Setting $2T$ to $1/J_{SS}$ = 28 ms for carbons will result in different signs for resonances of carbons coupled to odd and even numbers of carbons. On the other hand with $2T = 2/J_{SS}$ (56 ms) all resonances will have the same sign. Transverse relaxation during $2T$ limits the general applicability of *ct* evolution sequences because in large proteins relaxation may severely reduce the signal intensity. If *ct* evolution cannot be used, the maximal evolution time for heteronuclei with homonuclear couplings should not exceed $(4J_{SS})^{-1}$ which for aliphatic carbons corresponds to about 8 ms. This short maximal evolution time avoids the measurement of data with inherently low sensitivity caused by the cosine modulation of the signal due to the J_{SS} coupling. In addition linewidths cannot be significantly improved with longer evolution times since the unresolved homonuclear couplings can only be resolved using very long evolution times.

4.5.2 Concatenating basic segments

Generally, basic segments are implemented into pulse sequences by applying them consecutively as in the HSQC or HMQC experiments above or in a more complex example in Fig. 10. Although this results in a functional pulse sequence in some situations adjacent segments can be combined into a new segment. Such a concatenation may reduce the overall duration and/or the number of *rf* pulses and hence usually improves the sensitivity of the experiment. When evolution segments containing 180^o *rf* pulses (Fig. 11 and Fig. 12) occur consecutively such an optimization can often be performed [213]. Fig. 26 illustrates the procedure with some very frequently applied optimizations.

One combination of basic segments that frequently occurs in heteronuclear experiments consists of an evolution due to the chemical shift followed by an evolution due to J coupling to prepare a subsequent coherence transfer step (Fig. 26A). These two segments can be combined by reducing the number of 180^o *rf* pulses from three to two (Fig. 26A'). An algorithm that supports the optimization of pulse sequences has been developed [213] which is based on the properties of 180^o *rf* pulses. A 180^o pulse reverses evolution due to chemical shift and it also reverses evolution due to J coupling when applied only to one of two coupled spins. Thus the effective time that the spins evolve can be calculated by summing together time periods before and after a 180^o pulse with different signs. Following this recipe the effective time period t_δ during which the spins I in Fig. 26A' evolve due to chemical shift can be calculated as indicated in Eq. (4.4). The duration of t_δ must be equal to the chemical shift evolution time t in the scheme in Fig. 26A. Similarly the effective evolution time t_J of the I spins due to J coupling to the S spins can be calculated (Eq. (4.5)). Comparing with the original segments in Fig. 26A the duration of t_J must be set equal to $2\tau_{IS}$.

$$t_\delta = T_{A1} + T_{A2} - T_{A3} = t \tag{4.4}$$

$$t_J = T_{A1} - T_{A2} + T_{A3} = 2\tau_{IS} \tag{4.5}$$

Although Eqs. (4.4) and (4.5) have an infinite number of solutions only solutions with minimal overall duration are of interest. One obvious solution is $T_{A1} = t/2 + \tau_{IS}$, $T_{A2} = t/2$ and $T_{A3} = \tau_{IS}$.

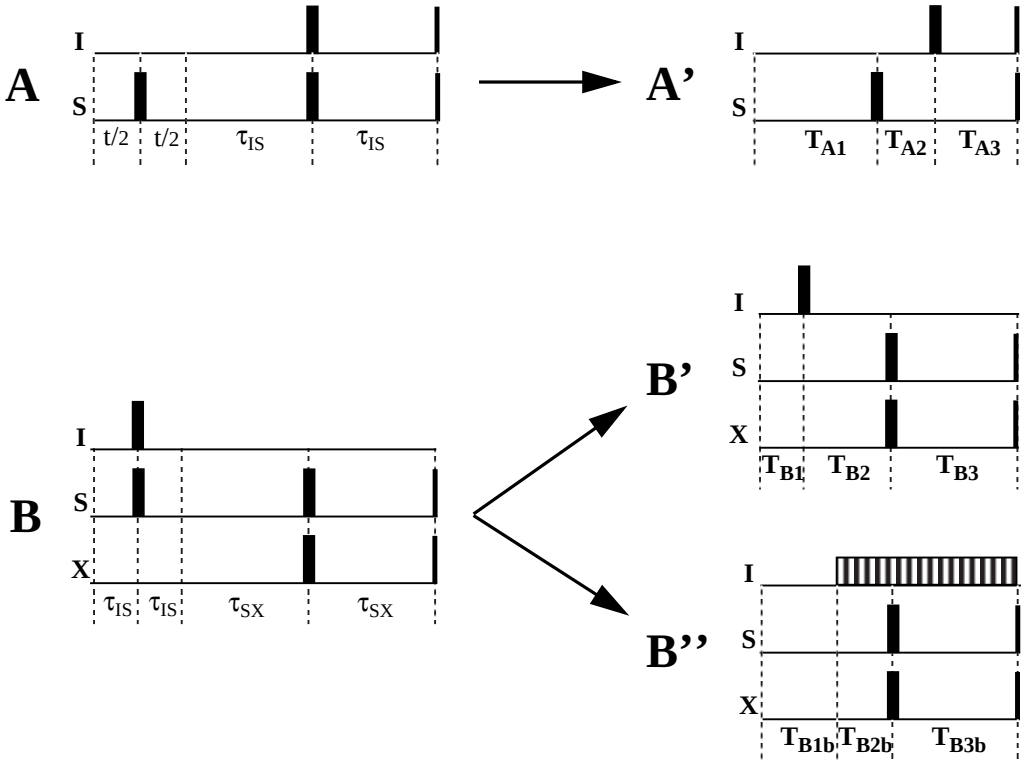

Fig. 26. Optimization of consecutively applied basic segments. (A) Time periods during which the spin states evolve due to chemical shift and due to scalar coupling are combined in (A') by reducing the number of 180° *rf* pulses. Depending on the boundary conditions used to calculate the time periods T_{A1}, T_{A2} and T_{A3} in (A') (see text) the duration of the segment to obtain the same spin state can be reduced compared to the original sequence. (B) Two consecutive time periods with effective evolution due to scalar coupling are combined in (B') and (B'') by reducing the number of 180° *rf* pulses and as well as the duration (see text). Two alternative schemes are presented: (B') using 180° pulses for decoupling of the *S* spins from the *I* spins and (B'') using a multipulse decoupling scheme.

Applying the pulse sequence in Fig. 26A' with theses values for the delays achieves the same result as the original sequence in Fig. 26A which uses one more 180° pulse.

In the solution just described the time t_J required for the INEPT transfer is not used for chemical shift evolution. A different solution of Eqs. (4.4) and (4.5) allows the use of the constant period $2\tau_{IS}$ for chemical shift evolution [214, 215] in multidimensional experiments. This scheme is often referred to as a semi-constant-time evolution period. The initial condition stays the same but now all three time periods are allowed to vary and T_{A3} should vanish for the last or *N*th increment of the evolution time. The following values describe a favourite solution, $T_{A1} = t/2 + \tau_{IS}$, $T_{A2} = t/2 - \tau_{IS}$ $(k-1)/(N-1)$ and $T_{A3} = \tau_{IS}$ $(N-k)/(N-1)$ where the integer k runs from 1 to N. This procedure does reduce both the number of 180° pulses and the overall duration of the sequence.

There is yet another solution of Eqs. (4.4) and (4.5) which finds frequent applications in pulse sequences used for heteronuclear multidimensional experiments. Setting the overall duration of the segment in Fig. 26A' to $2\tau_{IS}$ results in a scheme that allows chemical shift evolution which does not require any more time than required for evolution due to *J* coupling. Obviously in this case the chemical shift evolution time t is limited to a maximal value of $2\tau_{IS}$ or an odd multiple

thereof. This segment is usually referred to as a constant time evolution period. Solving Eq. (4.4) and (4.5) with these boundary conditions the time periods in the sequence in Fig. 26A' become $T_{A1} = t/2 + \tau_{IS}$, $T_{A2} = 0$ and $T_{A3} = \tau_{IS} - t/2$.

The successive application of polarization transfer steps is another very common combination of basic segments which can be optimized. In heteronuclear triple resonance experiments three nuclear species *I*, *S* and *X* are correlated. For example transverse *S* spin magnetization in anti-phase to *I* spins is refocused and subsequently let evolve into an anti-phase state with *X* spins (Fig. 26B). Optimization is achieved eliminating one 180° *rf* pulse to shorten the sequence. Again relations can be formulated [213] for the effective periods of evolution due to chemical shift, t_δ, the coupling between *I* and *S*, t_{IS}, and the coupling between *S* and *X*, t_{SX}. In the scheme in Fig. 26B only transverse magnetization of *S* spins is of interest. This magnetization should not exhibit evolution due to chemical shift as is formulated in Eq. (4.6). The required evolution due to *J* couplings results in Eqs. (4.7) and (4.8):

$$t_\delta = T_{B1} + T_{B2} - T_{B3} = 0 \quad (4.6)$$
$$t_{IS} = T_{B1} - T_{B2} + T_{B3} = 2\tau_{IS} \quad (4.7)$$
$$t_{SX} = T_{B1} + T_{B2} + T_{B3} = 2\tau_{SX} \quad (4.8)$$

When the scalar coupling J_{IS} between the *I* and *S* spins is larger than J_{SX} between the *S* and *X* spins a solution for Eqs. (4.6) to (4.8) is obtained with $T_{B1} = \tau_{IS}$, $T_{B2} = \tau_{SX} - \tau_{IS}$ and $T_{B3} = \tau_{SX}$. An alternative scheme (Fig. 26B'') uses a multipulse decoupling sequence instead of a 180° pulse to decouple the *I* and *S* spins during the additional time period the *S* and *X* spins require for an optimal coherence transfer. With $J_{IS} > 2J_{SX}$ one obvious solution is given by $T_{B1b} = 2\tau_{IS}$, $T_{B2b} = \tau_{SX} - 2\tau_{IS}$ and $T_{B3b} = \tau_{SX}$.

4.5.3 Sensitivity enhancement

Multidimensional NMR experiments contain among their basic segments several chemical shift evolution periods bounded by 90° *rf* pulses. The magnetization *M* entering the evolution period will be modulated by evolution due to chemical shift resulting in two orthogonal components, from which a subsequent 90° pulse will retain only one which does finally contribute to the measured signal. Therefore, increasing the dimensionality of a NMR experiment will generally decrease the sensitivity by $\sqrt{2}$. Further sensitivity losses occur when magnetic field gradients are used to select the magnetization of interest in the evolution time. Gradients select only one coherence level either positive or negative depending on the relative sign of the gradients (Eq. (2.30)). However, phase sensitive spectra require both levels to be retained in the coherence pathway. Hence when phase sensitive data are measured with gradient selection, two scans must be collected for each increment just as in a experiment using phase cycling. However gradient selection discards half of the signal resulting in an additional sensitivity loss of $\sqrt{2}$.

For certain classes of experiments pulse schemes have been developed that overcome the limitations described above and offer improvements in sensitivity. The sensitivity gains are realized by retaining both the cosine- and the sine-modulated components after the evolution time and transforming them into observable magnetization. A maximal sensitivity enhancement of $\sqrt{2}$ can be achieved for each indirect dimension using phase cycling for the coherence pathway selection and a maximal sensitivity enhancement of 2 using PFGs. The sensitivity enhancement schemes work best for heteronuclear two spin systems such as ^{15}NH and ^{13}CH moieties in isotope labelled

proteins [177, 216]. In cases where XH_2 and XH_3 moieties must also be detected, for example in proton-carbon correlation spectroscopy, the sensitivity enhancement is reduced [217]. In the following the application of a non-gradient, sensitivity enhanced INEPT segment to a two spin system is discussed, followed by a similar analysis of a sensitivity-enhanced INEPT segment using gradient selection.

The sensitivity enhanced sequences rely on a temporary "storage" of magnetization in a heteronuclear double quantum state. The pulse sequence segments in Fig. 27 are longer than the simple basic segments (Figs. 17A and 24A) and require more *rf* pulses. None the less a sensitivity enhancement can usually be obtained for small and medium sized proteins up to 25 kDa. Using

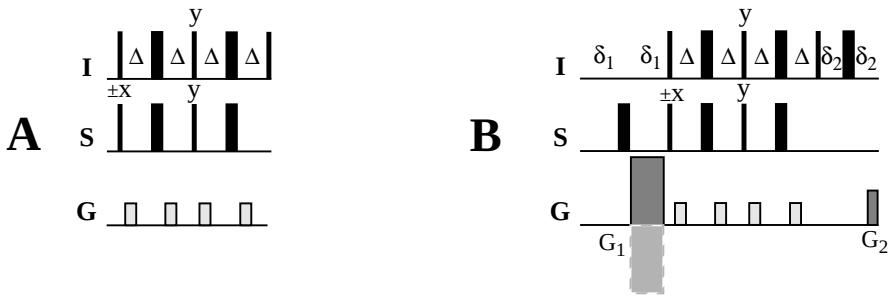

Fig. 27. Sensitivity enhancement schemes. All gradients except for G_1 and G_2 are applied to destroy potential artifacts caused by the 180° *rf* pulses. The delay Δ is set to $(4J)^{-1}$. (A) Both orthogonal magnetization components present after evolution of the *S* spins due to chemical shift are recovered. The coherence pathway is selected using phase cycling. (B) Scheme with gradient selection of the desired magnetization resulting in the same sensitivity as in (A). Concomitant with the phase change of the first 90° pulse on the *S* spins the sign of the gradient G_1 is changed. The gradients G_1 and G_2 must fulfil the equation: $G_1 = \pm\gamma_I G_2\tau_2/(\gamma_S\tau_1)$ where G_1 and G_2 are the respective gradient strengths and τ_1 and τ_2 the respective durations. The delays δ_1 and δ_2 are set to the duration of the gradient applied during these periods plus the necessary recovery delay.

the product operator formalism the principle of the enhancement sequences can easily be analysed. With the sequence shown in Fig. 27A the *S* magnetization in anti-phase to *I* spins present after a chemical shift evolution time t_e is transformed into detectable *I* magnetization [177] as follows:

$$2I_zS_y \cos(\Omega t_e) - 2I_zS_x \sin(\Omega t_e) \text{ ---> } \mp I_y \cos(\Omega t_e) - I_x \sin(\Omega t_e) \qquad (4.9)$$

where the phases of the first 90° pulse on *S* spins are x and –x. The two scans corresponding to these two phases must be stored in separate memory locations. Addition of the two scans produces the *x* component, $-2I_x \sin(\Omega t_e)$, and subtraction the *y* component, $2I_y \cos(\Omega t_e)$. After a 90° phase correction on one of the data sets the two data sets can be added resulting in a sensitivity enhancement of $\sqrt{2}$ since the conventional scheme only retains one of the two components. Gradients in the pulse sequence of Fig. 27A are only used to suppress potential artifacts from pulse imperfections.

Fig. 27B presents the sequence used to obtain a sensitivity enhancement of a factor of two in gradient selected multidimensional experiments [216]. For the gradient selection the strength of the gradient G_1 with duration τ_1 applied to transverse *S* spin magnetization and the strength of the gradient G_2 with duration τ_2 applied to transverse *I* magnetization must fulfil the relation

$G_1 = \pm\gamma_I G_2\tau_2/(\gamma_S\tau_1)$ (Fig. 23B). The additional small gradients in the sequence suppress possible artifacts. Just as with the non-gradient version this experiment requires, together with a sign change of gradient G_1, phase cycling of the first 90° pulse on *S* spins using the phases x and –x in alternating scans which are stored in separate memory locations. The sequence transforms anti-phase *S* spin magnetization present after an evolution time into detectable *I* spin magnetization according to

$$2I_zS_y \cos(\Omega t_e) - 2I_zS_x \sin(\Omega t_e) \text{ ---> } \pm I_y \cos(\Omega t_e) - I_x \sin(\Omega t_e) \qquad (4.10)$$

Phase x for the first 90° pulse on the *S* spins leads to the plus sign for I_y and phase –x with simultaneous inversion of the gradient G_1 to the minus sign. Phase sensitive data is obtained by phase correcting one of the data sets by 90° followed by addition and subtraction of the two separately stored experiments. This experiment has a sensitivity enhancement of factor 2 compared to the conventional gradient selected experiment. In other words, the sensitivity enhanced gradient selected experiments for two spin systems are as sensitive as their sensitivity enhanced nongradient counterparts.

4.6 Artifact reduction

Experiments can suffer from two categories of artifacts: those introduced by the particular method applied and those introduced by technical limitations of the NMR spectrometer. Examples of the first category are the signal loss when gradient selection is used, the interference effects due to insufficient relaxation delays between measurements and signal losses or artifacts due to the non-ideal excitation profiles of perfectly homogeneous *rf* pulses with limited power. Examples of the second category are artifacts introduced by the *rf* inhomogeneity of the pulses, instrumental instabilities, and artifacts introduced due to the huge dynamic range of proton resonances in a sample with a protein dissolved in H_2O. Numerous artifacts and remedies for their suppression have been discussed in the preceding sections. Most techniques which suppress artifacts rely on proper phase cycling of the *rf* pulses and the suitable application of magnetic field gradients. Effective use of these tools has lead to a very good average quality for multidimensional NMR spectra of proteins in aqueous solution. In this section a few additional frequently used procedures shall be presented. However, generally the basis for minimal artifacts remains a well maintained, state of the art NMR spectrometer in a stable environment [138].

The additional pulse sequence elements shown in Fig. 28 destroy selected magnetization components and may help to reduce artifacts. The elements in Fig. 28A and B make use of the inhomogeneity of the *rf* field to destroy unwanted magnetization components during a long spin-lock purge pulse [77]. Typically a 2 ms spin-lock pulse with a strength of about 15 kHz will completely destroy the water magnetization of a H_2O solution. During the spin-lock pulse all magnetization components not lying along the spin-lock axis are dephased and no longer produce a net signal. However, exactly as in the case of static pulsed magnetic field gradients (Section 4.4) zero quantum states present during the spin-lock pulse cannot be destroyed. The spin-lock field defines a magnetic field axis in the rotating frame around which the magnetization components precess during the pulse. Homonuclear anti-phase I_yS_z magnetization in the laboratory frame will represent a superposition of zero and double quantum states in the rotating frame of the spin-lock field applied along the *x* axis. Consequently half of the I_yS_z anti-phase magnetization will survive a spin-lock purge pulse with phase x. In Fig. 28B a second spin-lock pulse with phase y is included after a delay τ. This scheme destroys magnetization with arbitrary phase, such as the

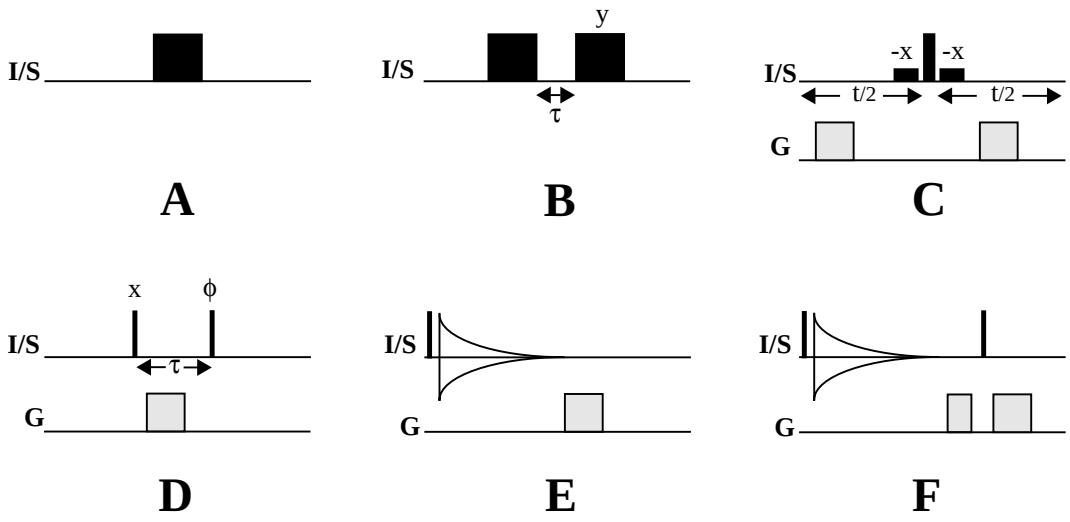

Fig. 28. Schemes used for the suppression of artifacts. (A) and (B) present spin-lock pulse elements which destroy magnetization due to the *rf* inhomogeneity of the applied *rf* field. (C) is a sequence that destroys resonances in a small spectral range, for example the water resonance. (D) shows a *z* filter that allows purging of undesired magnetization components. (E) and (F) depict schemes that destroy magnetization after the acquisition and eliminate interference effects between successive scans.

solvent resonance, which is on-resonance with the frequency of the two spin-lock pulses. Magnetization spin-locked by the first pulse precesses dependent on the offset Δ from the carrier frequency. The components which have rotated to align along the *y* axis survive the second spin-lock pulse. The intensities of all the resonances in the spectrum will be modulated by $\sin(2\pi\tau\Delta)$ with Δ being the frequency offset of a particular resonance from the carrier frequency. The period τ can be adjusted to have maximum excitation in the desired spectral range. In practical applications the length and power of the spin-lock purge pulses are limited by the specifications of the probe. If spin-lock purge pulses and PFGs are applied in a single pulse sequence, interference effects may occur [218] which degrade the performance.

A further solvent suppression scheme can be obtained by a combination of PFGs and selective excitation as shown in Fig. 28C. The 180^o pulse refocuses all magnetization with the exception of a small spectral region which is selectively excited by the two flanking 90^o low power pulses producing an effective 0^o pulse in this spectral region. Only magnetization that experienced an effective 180^o pulse refocuses due to the second gradient (Fig. 22C) whereas the signals in the narrow spectral region are destroyed. The duration *t* is kept as short as possible and typically does not exceed a few milliseconds. This sequence, known under the acronym WATERGATE [87], gives very efficient water suppression but at the same time strongly attenuates signals close to the water resonance. This limitation does not affect ^{15}N-relayed heteronuclear experiments where only amide protons are detected during acquisition. In such experiments the sequence can be integrated into the final INEPT step without lengthening the experimental scheme.

Fig. 28D displays a purging scheme known as *z* filter [219]. The magnetization of interest is taken through a *z* state so that the magnetization components remaining in the transverse plane can be destroyed by a PFG. Alternatively the phase of the second pulse and the receiver can be

incremented by 90^o in four successive scans. Of course, zero quantum coherence present during τ cannot be removed by this element. However in analogy with the NOESY sequence the time τ can be incremented or randomized between successive scans to suppress zero quantum states based on their precession during τ. When relaxation permits, an improvement of *z* filters and trim pulses can be obtained by spin-locking with inhomogeneous B_o or B_1 fields, a technique which can also achieve dephasing of zero quantum states [220].

The repetition rate of pulse sequences in a typical NMR experiment must be a compromise between reaching the Boltzmann equilibrium at the start of the sequence and an efficient signal acquisition requiring relatively short interscan delays. Typically, interscan delays are between one and 1.5 seconds which is often too short to reach thermal equilibrium. The spectra are measured in a steady state mode which can lead to interference effects in successive scans resulting in artifacts in the final spectrum. For example, in COSY spectra small resonances on a line with double the slope of the normal diagonal can sometimes be observed. These artifacts originate from resonances which have not fully relaxed between two scans and hence were frequency labelled a second time obtaining double the frequency in the indirect dimension. With the scheme presented in Fig. 28E all transverse magnetization can be destroyed after the acquisition. This is often not of prime interest for protein resonances which usually have a fast enough transverse relaxation not to cause interference, however the procedure may be useful for small molecules and peptides. In cases where interference effects are transmitted *via z* states not only resonances of small molecules but also protein resonances may contribute. Fig. 28F shows a sequence based on magnetic field gradients that destroys all magnetization after the acquisition and guarantees identical starting conditions for all scans during an experiment. Alternatively, this sequence can be replaced by the element shown in Fig. 28B with τ set to zero.